The analysis of zebrafish meiotic mutant *ietsugu* which shows critical decrease of *sycp2* expression

TAKEMOTO KAZUMASA

Doctor of Philosophy

Department of Genetics
School of Life Science
SOKENDAI (The Graduate University for Advanced Studies)

The analysis of zebrafish meiotic mutant *ietsugu* which shows critical decrease of *sycp2* expression

Takemoto, Kazumasa

DOCTOR OF PHYLOSOPHY

Student ID 20131802

Department of Genetics

School of Life Science

SOKENDAI

(The Graduate University for Advanced Studies)

2017

Contents

Pages

1. Abstract

Meiosis is special cell division that halves chromosome numbers from diploid into haploid. To achieve this drastic change, meiocytes express various meiotic chromosomal proteins in addition to mitotic chromosomal proteins. By these meiotic chromosomal proteins, chromosomes in meiosis show meiosis-specific architectures, telomere bouquet on inner nuclear membrane (INM), chromosome axis between sister chromatids, and synaptonemal complexes (SCs) between homologous chromosomes. Although the meiotic chromosomal proteins are divergent between vertebrates and invertebrates, defects in these proteins result in disruption of meiotic chromosomal architecture leading to sterility. Taking the fact that many meiotic proteins required for SC formation in vertebrates are well conserved, understanding the function of these proteins in a model vertebrate should be important for fertility clinic of humans. However, despite many studies of meiotic chromosomal proteins, the detail structural role of those proteins in the architecture of meiotic chromosomes remains to be elucidated.

In this study, I analyzed a zebrafish meiotic mutant, *ietsugu* (*its*), that was generated by an N-ethyl-N-nitrosourea (ENU) mutagenesis and shows a defect in meiotic chromosome architecture. Previous study in our laboratory identified that the mutation of the *its* mutant was linked to a locus in chromosome 23 which contains two chromosomal genes, synaptonemal complex protein2 (*sycp2*) which is meiotic protein, and *smc1al* which is global chromosomal protein. However, no mutation was found in those ORFs. Both Sycp2 and Smc1al are structural protein related to SCs. RT-qPCR of these genes revealed that the amount of *sycp2* transcripts in the *its* mutant was 80 %

lower than that in WT sibling, while the amount of *smc1al* transcripts in the *its* mutant and WT was the same. A knockout (KO) of *sycp2* generated by TALEN resulted in sterility due to meiotic arrest at prophase I similarly to the *its* mutant. By the complementation test using *sycp2* KO and the *its* mutant revealed that *sycp2* KO did not complement the sterility of the *its* mutant. Furthermore, immunohistochemistry and fluorescence in situ hybridization (FISH) to visualize telomeres revealed that synapsis from telomere bouquet by the Sycp1 protein was completely disrupted in *sycp2* KO, while it was maintained in the *its* mutant. Sycp3, the other protein which acts together with Sycp2 as SC protein showed large nuclear aggregates in both the mutant and the KO. These finding strongly suggest that the *its* mutant is a hypomorphic mutant of *sycp2*. The *sycp2* cDNAs cloned from the *its* mutant revealed that there are normal and aberrant transcripts of *sycp2* the latter of which that contains a 5 bp insertion making termination site. The ratio of normal *sycp2* mRNA was only 10% in the *sycp2* transcripts of the *its* mutant compared to WT. Genomic sequencing revealed that the intron 8 of the *its* mutant contains a T to A conversion that can work as aberrant 3'-splice site. Forced expression of minigene containing intron 8 of the *its* mutant in WT fish also showed mis-splicing. This suggests that this aberrant splicing is independent of genetic background. By immunohistochemistry, western blotting analysis and immunoprecipitation, I could not detect the Sycp2 protein in testes of the *its* mutant. These suggest that, in the *its* mutant, the amount of the Sycp2 protein is extremely low. Thus, I interpreted that the responsible mutation in the *its* mutant is the T to A substitution at intron 8 that makes aberrant splicing products leading to extremely low expression of Sycp2. Additionally, immunohistochemical analysis of Sycp2 in WT revealed that Sycp2 did not co-localize with Sycp3 in preleptotene while

these proteins began to co-localize from leptotene. This suggests that Sycp2 is required for re-localization of Sycp3 from aggregate to SCs.

Synapsis from telomere bouquet in the *its* mutant could be resulted from low amount of Sycp2 and self-assemble property of Sycp1 that can form SCs-like structure even in *sycp2* KO.

Therefore, I conclude that the *its* mutant is a hypomorphic mutant of *sycp2* that show maintenance of the association of the tips of SCs and telomeres. Also, using the *its* mutant, I revealed that association of the tips of SCs with telomere on INM requires specific meiotic chromosomal protein Sycp2. This clearly indicates the new aspect of meiotic chromosome architecture in vertebrates and that is association of telomere and the tips of SCs is different phenomenon with attachment of telomeres on INM because attachment of telomeres onto INM requires other proteins. This also indicates the new role of Sycp2, which was thought to be just a component of SCs, to associate the tips of SCs and telomeres.

2. Introduction

Chromosomal architecture in meiosis prophase-I requires many proteins in addition to mitotic ones. Both mitosis and meiosis requires cohesin complexes to form chromosome cores and meiosis additionally requires meiosis-specific cohesin subunits (Bannister et al., 2004; Xu et al., 2005; Revenkova et al., 2004). Furthermore, meiocytes show the most prominent structures in meiotic chromosome architectures, Synaptonemal complexes (SCs) (Fraune et al., 2012) and tethering telomere onto inner nuclear membrane (INM) (for a review, see Shibuya and Watanabe, 2014). The correct chromosome architecture and the dynamics in meiotic prophase I is crucial for fertility (Fraune et al., 2012). Meiosis prophase I is classified into several stages based the dynamics of chromosomes (Fig. 1A). Following the premeiotic S phase, spermatocytes enter into the preleptotene stage. In this stage, telomeres attach to INM via attachment plates (Liebe et al., 2004). After the attachment of telomeres to INM, spermatocytes enter into the leptotene stage. In this stage, especially in late leptotene, telomeres form cluster in one pole of nucleus, thich is called telomere bouquet (Chikashige et al., 1994; Scherthan et al., 1996). At the same time, chromosome axes start to be formed in each chromosome. These axes are proteinaceous structure called axial elements (AEs) composed of its specific proteins and cohesins (Rong et al., 2016). The tips of AEs in late leptotene are connected to telomeres. Several specific proteins associated with telomere bouquet have been identified. Loss of those factors results not only in detachment of telomeres from INM but also in defective chromosome architecture and sterility (For a review, see Shibuya and Watanabe., 2014). Interestingly, in these cases telomeres always associate with the tips of AEs (Shibuya et al., 2015).This suggests that the association of the tips of SCs is different phenomenon with attachment of telomere

to INM. Next, in zygotene stage, homologous chromosomes start to synapse each other facing their AEs via transverse filaments (TFs) and central elements (CEs). After the synapsis of homologous chromosomes, AEs are called lateral elements (LEs). This tripartite structure composed of AE/LEs, TFs and CEs is called SC. In the late zygotene stage, telomere bouquet is dissolved and telomeres disperse in nucleus attaching to INM. Finally, spermatocytes with fully synapsed homologous chromosomes via SCs are in the pachytene stage. Thus, SCs are formed between homologous chromosomes supported by connection of AE/LEs and telomeres on INM.

Many KO studies of meiotic cohesin subunits (Xu et al., 2005) and components of SCs (Fraune et al., 2012) in rodent models provide basic knowledge for meiotic chromosome architecture. These studies show that the lack of meiotic cohesin subunits, components of SCs and meiotic telomere factors result in male infertility. Among them, KOs of SCs components show drastic defects on meiotic chromosome architecture and phenotypes of the KOs are completely different. For TFs, only SYCP1 is known (Meuwissen et al., 1992). For CEs, synaptonemal complex central element 1, -2, -3 (SYCE1, -2, -3), testis expressed 12 (TEX12) and C14ORF39/SIX6OS1 (Fraune et al., 2012; Gómez-H et al., 2016) are known. Homozygous mutants or KOs of TF or CE proteins result in sterility by arrest of meiosis in zygotene-pacytene stage due to synaptic defect while heterozygous mutants are fertile. The phenotype is restricted to synapsis and no defect was observed in AE/LEs formation (For a review, see Fraune et al., 2012; Gómez-H et al., 2016). For AE/LEs which directly connect to telomeres, SYCP2 and SYCP3 are known and these KOs results in sterility (Yuan et al ., 2000; Yang et al., 2006). Interestingly, these proteins show different dynamics for telomeres in KOs of their counterpart. When SYCP2 does not exist, SYCP3 form large aggregates

which do not co-localize with telomeres and SCs-like structure marked by SYCP1, (Fig. 2; *Sycp2* KO) (Yang et al., 2006). In this case, the SCs-like structure also detach from telomeres (Fig. 2; *Sycp2* KO). On the other hand, when SYCP3 does not exist, SYCP2 form thread- or dot-like foci that often co-localize with telomeres (Fig. 2; *Sycp3* KO) (Yuan et al ., 2000; Liebe et al., 2004). Also in this case, the SCs-like structure detach from telomeres (Fig. 2; *Sycp3* KO) (Liebe et al., 2004). These results indicate that SYCP2 is required for localization of SYCP3 onto SCs as AE/LEs. In the case of double KO of *Sycp1* and *Sycp3*, telomeres can attach onto INM and the localization pattern of SYCP2 is same as *Sycp3* KO (Kouznetsova et al., 2011). Therefore, it is indicated that in AE/LEs proteins SYCP2 is only protein which can access to telomeres independent of other proteins. The attachment of telomeres onto INM is also important for proper synapsis because the disruption of tethering proteins of telomeres onto INM result in aberrant synapsis and sterility (For a review, see Shibuya and Watanabe., 2014). Thus, INM-telomere-SC connection is important for meiotic chromosomal architecture and proper gametogenesis. SYCP2 seems to be critical part for connection between telomeres and SCs (Liebe et al., 2004).

SYCP2 has 1500 amino acids and was first identified in rat by cDNA screening (Offenberg et al., 1998). SYCP2 has coiled-coil domain in C-terminal region and rich in β -turns. N-terminal region has limited similarity with budding yeast SCs protein Red1. SYCP2 also has several short amino acid sequence motifs, S/T-P DNA binding sites, cAMP/GMP kinase target sites and $p34^{cdc2}$ kinase target sites. From these, Offenberg et al. (1998) speculated that SYCP2 is a DNA binding protein which is involved in meiotic chromosome architecture. Recently, the in vitro study by Feng et al. (2017) showed that the N-terminal region also has armadillo-repeat-like domain (ARLD) and Spt16M-like

domain (SLD). They also showed that ARLD can interact with centromere proteins CENP J and CENP F by yeast two hybrid system and co-transfection into COS-7 cells. SLD resembles to histone chaperone FACT. So, they speculate that SYCP2 has some role on centromere and histone. By the biochemical analysis, SYCP2 has a role to provide a link between SYCP1 and SYCP3 which do not interact with each other (Winkel et al. (2009).

Despite these studies, there is no evidence to show the actual role of Sycp2 on telomere in vivo probably due to the difficulty of observation on relationship between AE/LEs and telomeres in rodent models. Generally in rodents, formation of AEs which start from leptotene stage spreads throughout nucleus and Sycp2 always co-localizes with Sycp3 (Llano et al.,2012; de la Fuente et al., 2007; Judis et al., 2004). In addition, the frequency of the cells undergoing telomere bouquet stage in mice is quite low (Liebe et al., 2006). The study about relationship between AE/LEs and telomeres is clinically important for treatment on infertility in human because the mutations in components of SCs result in infertility (Bolcun-Filas et al., 2009; Judis et al., 2004; Bolor et al., 2009). Although many studies about relationship between AE/LEs and telomeres have been performed in other non-vertebrate model organisms, their SC proteins have less similarity with vertebrate lineage ones, and the numbers of SCs components, especially of AE/LEs, are also different from vertebrate lineage (For a review, see Fraune et al., 2014,Cahoon and Hawley, 2016 , Cahoon et al., 2017; Hawley, 2011; Lui and Colaiácovo, 2013; Woglar and Jantsch, 2014) Therefore, to assess the functions of AE/LEs proteins in vertebrates toward clinical treatment for human infertility, another appropriate experimental approaches are required.

Among the vertebrate models, teleost models such as zebrafish and medaka show different characteristic chromosome dynamics and SCs formation from rodents(Fig. 1B) (Iwai et al., 2006; Saito et al., 2011). After the bouquet formation in leptotene, AEs start to elongate from one pole of nuclei where the bouquet exists. Soon after elongation of AEs, synapsis starts from bouquet (Saito et al., 2014). Interestingly, it is also reported that synapsis initiates at subtelomeric regions in human male spermatocytes (Brown et al., 2005; Gruhn et al., 2016). This property of synapsis resembles that of zebrafish. Therefore, the characteristic chromosomal dynamics of zebrafish are strong advantages to understand the molecular cascade of vertebrate meiotic chromosome architecture especially in relation to telomeres and SCs in vertebrates including human.

Previously, several zebrafish meiotic mutants which show sterility due to meiotic arrest at prophase I have been isolated from ENU mutagenesis screening on male gonadogenesis (Saito et al., 2011). Among them, the *its* mutant shows the characteristic phenotype of severe aggregation of Sycp3 protein in nucleus. The causal genomic locus was successfully narrowed down into chromosome 23, (Saito, unpublished data) however, no mutation was found in ORFs of genes in the locus. I speculated that the *its* mutant has mutation related to meiotic gene expression level in causal genomic locus of chromosome 23, especially the ones related to meiotic chromosome architecture.

In this thesis, I first analyzed the expression level of *sycp2* in the *its* mutant. Second, I established TALEN-induced KO fish of *sycp2* (*sycp2* KO) to perform complementation test and to compare the meiotic chromosome architecture of *sycp2* KO with the *its* mutant by histological and cytological analysis of Sycp1, Sycp3 and telomeres. Finally, I identified the causal mutation in the intron 8 of *sycp2* by cDNA cloning and the minigene assay. Furthermore, I analyzed the dynamics of the Sycp2 protein by

immunohistological analysis to assess its role in meiotic chromosome architecture. This study presents that low expression level of *sycp2* affect fertility and meiotic chromosome architecture involving telomeres differently from straight KO.

3. Materials and Methods

Fish Maintenance

Zebrafish (*Danio rerio*) were maintained under standard conditions as described (Westerfield, 1995). Wild-type strain was obtained from Dr. N. Hopkins (Center for Cancer Research, Massachusetts Institute of Technology). The *its* mutant was isolated from mutant collection from Dr. K.R. Siegfried (Saito et al., 2011). The use of zebrafish for experimental purposes was conducted in accordance with the guidelines of the National Institute of Genetics (An approval number; 24-12).

Caudal fin clip and lysis

Adult zebrafish were anesthetized by 0.2 mg/ml 3-aminobenzoic ethyl ester. After anesthetization, caudal fin was clipped by clean scalpel and digested by 100µl of lysis buffer (200µg/ml proteinase K,10 mM Tris-HCl pH 8.0, 1mM ethylenediaminetetraacetic acid (EDTA), 0.1% Nonidet P-40) in 65℃ for overnight. After digestion, lysates were diluted into 1/120 by water and used for genotyping.

Sample preparation for histological analysis

Testes from adult zebrafish were fixed in Bouin's solution at 4℃ overnight (Bouin's solution: saturated picric acid 15 ml, 40% formaline 5 ml, acetic acid 1 ml). Fixed testes were dehydrated by ethanol series (70%, 80%, 90%, 100%), methyl benzoate and Lemosol (Wako, Japan). After dehydration, testes were embedded in paraffin, and sectioned at a thickness of 5 µm using rotary microtome 2065 Supercut (Leicamicrosystems Co.Ltd., Tokyo, Japan). Sections were pasted on micro slide glasses (Matsunami Glass Ind Ltd., Osaka, Japan) and dried for overnight.

cDNA synthesis

The total RNA from 3 fin clips or a pair of testes were isolated using RNAiso Plus (TaKaRa, Japan) according to manufacturer's protocol. The total RNA was treated by TURBO DNase (Ambion) according to manufacturer's protocol, and then re-extracted with RNAiso Plus to eliminate remaining DNA.

One μg of total RNA was reverse-transcribed into cDNA using PrimeScript RT-PCR kit (TaKaRa) according to manufacturer's protocol. Oligo dT primer was used in the reverse-transcriptions.

RT-qPCR

RT-qPCR of testis cDNA was performed on LightCycler480 system (Roche) using LightCycler480 SYBR Green I Master according to manufacturer's protocol. For PCR cycles, annealing temperature was set at 58℃ and other settings were set to default values. Primers used for RT-qPCR were shown below. All primers were designed to amplify 3' sides of ORF.

sycp3-F; 5'-GCTGAGCAAGAAAAGATCTGC-3'

sycp3-R; 5'-TTTTTGGTGAGAACCTCCAG-3'

for *sycp3*;

sycp2-F; 5'-AGTTCTCAGAGGTTGGAGAAAGT-3'

sycp2-R; 5'-TCTCTTGGTAGGTGTGGAAGG-3'

for *sycp2*;

rps29-F; 5'-CGATCGAGAGAGACGAGATG-3'

rps29-R; 5'-GGCACATGTTGAGTCCGTATT-3'

for *rps29*;

sycp1-F; 5’-GCAGAGCTGAGTGAAAAACG-3’

sycp1-R; 5’-TGACACTGGTGTCTTCAGGA-3’

for *sycp1*;

bactin1-F; 5’-CAATGAGCGTTTCCGTTGC-3’

bactin1-R; 5’-ACCGCAAGATTCCATACCCA-3’

for *bactin1*;.

To quantify the retention of intron3 in *sycp2* transcripts in the *its* mutant and *sycp2* KO, primers shown below were used;

sycp2-spliced-F; 5’-TGTTAAAAAGCTGGTGCAGTG-3’

sycp2-spliced-R; 5’- AACTTTCATGGACAACCATCAG-3’

for intron3 spliced form of *sycp2*;

sycp2-retained-F; 5’- TGTGTATGTACCTGGTGCAGTG-3’

sycp2-retained-R 5’- CTTCTTTGCAACTTTCATGGAC-3’

for intron 3 retained form of *sycp2*;.

Design of TALEN and generation of *sycp2* knock out zebrafish

TALEN was designed to target zebrafish *sycp2* exon18 using TALEN Targeter (Doyle et al., 2012). Each parameter was set shown below; minimum spacer length and maximum spacer length were 15 bp, minimum repeat array length and maximum repeat array length were 15 bp, G substitute was NN and upstream base was T only. All other parameters were set to default values. Resulting Target site for left TALEN was 5’-TGATGAAGCCAGCTCT-3’ and for right TALEN was 5’-GTGTCTCTCCTTCTTT-3’. The TALEN vectors were constructed using Golden

Gate assembly method (Cermak et al., 2011; Sakuma et al., 2013). TALEN mRNA was transcribed using mMessage Machine SP6 kit (Ambion) according to manufacturer's protocol. About 1 ng of synthesized mRNA was injected into 1-4 cell embryos of WT India strain. Injected male fish was mated with other India strain and sibling was genotyped by PCR and sequencing using caudal fin lysate and following primers: F-primer; 5'-TTCAAAGCCAATGATGAAGC-3' and R-primer; 5'-CGAAGCTCAATCTCTTTCTTCC-3'. Finally, sibling containing same deletion was inbred to obtain homozygous KO fish.

Complementation test

Heterozygous mutant of *its* (sycp2 $^{its/IM}$) was genotyped by genomic PCR using simple sequence length polymorphism (SSLP) marker in chromosome 23, z20895 primer pair (Primer A: 5'-CAACACAACCCACAGTCAGG-3' and Primer B: 5'-CCCACCCCCTACTCAAAAA-3') and z7550 primer pair (Primer A: 5'-CGATCCCTTCGTTTGTTGTT-3' and Primer B: 5'-TGCTCAAGTCTTTTCCTCCTG-3'). IM strain is WT inbred strain (Shinya and Sakai, 2011). The heterozygous *its* mutant (sycp2 $^{its/IM}$) was crossed with *sycp2* heterozygous KO (*sycp2* $^{KO/India}$). To obtain the offspring containing *its* and *sycp2* KO allele (*sycp2* $^{KO/its}$), the offspring were genotyped by PCR shown above (see Design of TALEN and knock out of *sycp2*) at first. Then, the offspring containing *sycp2* KO allele (*sycp2* $^{KO/IM}$ or *sycp2* $^{KO/its}$) were re-genotyped by PCR using z20895 primer pair, and offspring containing *its* allele and KO allele (*sycp2* $^{KO/its}$) were obtained. Those offspring (*sycp2* $^{KO/its}$) were confirmed by genotyping using z7550 primer pair. The

male from those offspring were used for the observation of testicular phenotype and crossed with WT female to examine their fertility.

Construction of the minigene

To construct the minigene, genomic *sycp2* fragments spanning exon8 to exon9 were amplified by PCR using KOD –Multi & Epi- (TOYOBO, Japan) using primer pair containing restriction sites (F primer; 5'-TTTAAGCTTATGATTGGTGTGGCCTGTCGAATC-3' and R-primer; 5'-TATGGATCCCCAGTTTCAAACTCAGAATCCTTGATC-3') from WT India genome and *its* homozygote genome. The PCR products were digested with *Hind*III and *Bam*HI, and cloned into the pT2AL200R150G (Urasaki et al., 2006) vector's *Hind*III and *Bam*HI sites. Each construct was sequenced to check restriction sites, codon frame and splice sites of intron 8. Finally, these constructs were purified using Nucleospin Easypure (Machrey-Nagel) , and injected into WT India strain embryos at 1-4 cell stages with transposase mRNA (Kawakami et al., 2004) to generate transgenic (Tg) zebrafish of the minigenes .

RT-PCR and cloning of *sycp2* cDNA fragments.

Testicular total RNA and fin total RNA were purified and reverse-transcribed into cDNA as shown above. cDNA fragments were amplified by PCR using KOD –Multi & Epi- using primers shown below. *sycp2* cDNA is 4710bp. To amplify 5' side (1-1508 bp), internal area (1487-3085 bp) and 3' side (3011-4710 bp), primer pairs were designed as following.

1-1508F; 5'-ATGGCACCTTTGCAGGACCATC-3'

1-1508R; 5’-GCTGGCTTCATCATTGGCTTTGA-3’

1487-3085F; 5’-CAAAGCCAATGATGAAGCCAGCTC-3’

1487-3086R; 5’-TGGTTGTGTCCACAGAGGGTTTTTG -3’

3011-4710F; 5’-CGCCTCAGGAGATTGTTTCAGC-3’

3011-4710R; 5’-TCAGAACCTGGATGCATCTGGAAAG-3’

To amplify 1st ATG to exon9 of *sycp2* from testes total RNA, primer pair was used as following.

1-684F; 5’-ATGGCACCTTTGCAGGACCATC-3’

1-684R; 5’-CATTCTGCAGAGGGCCTCCATT-3’

To amplify exon1-3, exon3-5, exon4-6, primer pairs were used as following.

Exon1-3F; 5’-ATGGCACCTTTGCAGGACCATC-3’

Exon1-3R; 5’-GCATGGTCCACATTTCCAACC-3’

Exon3-5F; 5’-ATGGTTGCGCAGGGATTTGT-3’

Exon3-5R; 5’-CCTTCTTTGCAACTTTCATGGACA-3’

Exon4-6F; 5’-GAGGCAGGGCCATCAAAAA-3’

Exon4-6R; 5’-GGCATCAGAAGCCAGTTTGC-3’

To amplify junction between exon8 and exon9, primer pairs were used as following.

60bp F; 5’-CCTGTCGAATCCTCAAAGGT-3’

60bp R; 5’-AGAGGGCCTCCATTAAAGAC-3’

70bp F; 5’-ATGATTGGTGTGGCCTGTC-3’

70bp R; 5’-GGGCCTCCATTAAAGACACT-3’

For a control to distinguish Tg of minigenes with non-Tg fish by existence of EGFP, primer pair was used as following.

EGFP up; 5’-ACCACATGAAGCAGCACGACT-3’

EGFP down; 5’-CTTCTCGTTGGGGTCTTTGC-3’

Amplified fragments were adenylated using LA Taq (TaKaRa) and cloned into pGEM-T easy vector (Promega) using Ligation high ver.1 (TOYOBO) according to manufacturer’s protocol.

Sequencing analysis

Genomic locus of exon 8 to 11 of zebrafish *sycp2* was amplified by PCR using KOD – Multi & Epi- (TOYOBO). Forward primer was exon8-F; 5’-GATTGGTGTGGCCTGTCGAA-3’. Reverse primer was exon11-R; 5’-TTTTTCCAAAAACGCCTCTA-3’. Amplified DNA fragments were treated by 5 μl of Exo-SAP, which was diluted into 1/20 with water at 37℃ for 3 hours followed by heating in 80℃ for 15 min.

Purified genomic PCR fragments were sequenced using same primer shown above. pGEM-T vector containing *sycp2* fragments were sequenced using T7 or SP6 primer. For sequencing, BigDye terminator v3.1 cycle sequencing kit (Applied Biosystems) was used.

Generation of polyclonal antibody against Sycp2

For the antigen to generate polyclonal antibody, recombinant Sycp2 protein was prepared from bacterial expression system. cDNA fragments coding C-terminal 499 amino acid residue without termination codon of Sycp2 (Sycp2C499) was amplified by RT-PCR using primers with BamHI site (Sycp2C499BamHI-F; 5’-ATAGGATCCTGGGACAGACAGAAAGAAACC-3’) and with XhoI site (Sycp2C499XhoI-R ;5’-TTTCTCGAGGAACCTGGATGCATCTGGAA-3’). After

digestion of fragments by *Bam*HI and *Xho*I, fragments were subcloned into pET-21a vector (Merck Millipore) with C-terminal sequence coding 6x histidine tag. Recombinant Sycp2C499 was expressed in *E.coli* Rosetta-gami2 (DE3) strain (Merck Millipore) by induction of the Sycp2C499 expression using isopropyl beta-d-thiogalactopyranoside (IPTG) and purified using Ni-NTA agarose (QIAGEN) according to manufacturer's protocol with slight modifications. Bacteria from cultured for 3.5 hour from IPTG induction were centrifuged and those pellets were suspended in 60 ml of lysis buffer A (100 mM NaH_2PO_4, 10 mM Tris-HCl, 6M guanidine hydrochloride, pH8.0) for overnight. Lysate were centrifuged to deplete cellular debris. Cleared lysate were incubated with 1.25 ml of Ni-NTA agarose beads for 2 hours with gentle mixing. Beads-lysate mixture was applied onto polypropylene column (QIAGEN) and beads were filtrated. Remaining beads were washed by buffer GC (100 mM NaH_2PO_4, 10 mM Tris-HCl, 6M guanidine hydrochloride, pH6.3) 3 times. Recombinant proteins bound to the beads were eluted by buffer GE (100 mM NaH_2PO_4, 10 mM Tris-HCl, 6M guanidine hydrochloride, pH4.5). Eluates were dialyzed for 2 days against PBS containing 1mM dithiothreitol at 4℃. Resulting suspension containing aggregates composed of the recombinant protein and other contaminated proteins were collected. The recombinant proteins were separated by SDS-PAGE using 10% acrylamide gel and other conataminants were depleted by coomassie brilliant blue staining and slicing gel. Sliced gel containing the recombinant protein were washed by water and crushed in PBS. Totally 500 μg of recombinant protein was immunized as antigen for 5 times into guinea pig (Evebioscience, Japan).

Serum was corrected after fifth injection of antigen. To purify the IgG from antiserum and normal guinea pig serum (Jackson Immunoreserch) for negative control, Protein-A

HP SpinTrap (GE healthcare) was used according to manufacturer's protocol. After the purification, concentration of both IgG was adjusted to 1mg/ml by 10 mM Tris-HCl solution (pH7.4) containing 1% BSA, 0.15M NaCl and 0.03 % Proclin 300 (Sigma-aldrich).

Immunoprecipitation

Two pairs of testes were mushed in 300 µl of RIPA buffer (50 mM Tris-HCl (pH8), 150 mM NaCl, 1% NP-40, 0.5 % sodium deoxycholate, 0.1 % SDS, protease inhibitor cocktail (WAKO)). The remained debris was depleted by centrifugation of 12,000 x g for 2 min. Supernatants were transferred into new microtubes. Those supernatants were precleared by incubating with 12 µl of protein-A sepharose (Roche) at 4℃ with mixing. These suspension were centrifuged by 3000 x g for 2 min at 4℃ and cleared supernatants were obtained. Cleared supernatants were divided into two microtubes and incubated at 4℃ for 1 h or overnight with 3 µg of guinea pig anti-Sycp2C499 antibody or normal IgG. After addition of 6 µl of protein-A sepharose, these suspension were incubated at 4℃ for 1 h with mixing. Protein-A sepharose were centrifuged and washed by 10 µl of RIPA buffer 3 times. Precipitated proteins were eluted by boiling of Protein-A sepharose for 10 min in 10 µl of 1 x sample buffer (69 mM Tris-HCl (pH6.8), 2.2% sodiumdodecylsulfate (SDS), 11 % glycerol, 0.05 mg/ml Bromophenolblue (BPB), 50 µl/ml 2-mercaptoethanol). 5 µl of eluted samples were used for SDS-polyacrylamide gel electrophoresis (SDS-PAGE) and western blotting.

SDS-PAGE and western blotting

A pair of testes was mushed in 140 µl of dyless 1 x sample buffer (sample buffer without BPB) and boiled for 10 mins. After boiling, lysate was vacuumed and pushed in 27 gauge needle and 10 ml syringe. After that, debris was depleted by centrifugation in 20,000 x g for 5 mins. Protein concentration of lysate was measured using 2D-Quant kit (GE healthcare) according to manufacturer's protocol. 10 µg of protein were applied on polyacrylamide gel in SDS-PAGE used for further experiment.

SDS-PAGE was carried out using a Tris-glycine buffer system (Laemmli et al., 1970). For western blotting, separated proteins on polyacrylamide gel were transferred to Immobilon-P membrane (Merck Millipore). Blotted membrane was blocked by 3% blocking reagent (Roche) in Tris-buffered saline (TBS; 20mM Tris-HCl, 137 mM NaCl pH 7.5) containing 0.1% Tween20 (TBST) at room temperature for overnight. Next day, the membrane was treated with guinea pig anti-Sycp2 antibody diluted into 1:1000 with CanGetSignal solution 1 (TOYOBO) for 1 hour at room temperature. After immunoreaction, membrane was washed by TBST 3 times. Next, the membrane was blocked by 5% skim milk (Wako) in TBST at room temperature for 1 hour. After blocking, membrane was treated with anti-guinea pig IgG antibody conjugated with alkaline phosphatase (AP) (SantaCruz) diluted into 1:1000 with CanGetSignal solution 2 (TOYOBO) for 1 hour at room temperature. After the 3 times of wash with TBST, presence of AP on membrane was visualized by treating membrane with NBT/BCIP stock solution (Roche) diluted into 1:100 with DigIII buffer (100mM Tris-HCl, 100 mM sodium chloride, pH 9.5 by hydrochloric acid). After staining, reaction was stopped by dipping the membrane in 1 mM EDTA solution.

Spermatocyte spread

Testes of zebrafish were removed and minced by scalpel on clean plastic petri dish. Minced testes were transferred to 1.5 ml microtube and were treated with 300 µl of 500U/ml collagenase in L-15 (SIGMA-ALDRICH) for 30 min. Every 10 minutes, minced testes were pipetted. Debris was depleted by filtration by using 40 µm nylon mesh. Filtrated cells were centrifuged for 30 mins in 100 x g and washed with PBS. The dissociated cells were suspended in 3 ml of PBS and 100 µl of suspension were placed onto MAS-coated slide glasses for 20 min. After that, suspensions on the slide glass were removed by micropipette and cells were spread by treatment of 85 mM NaCl solution for 15 mins. After spread, cells were fixed with 1% paraformaldehyde (PFA) in PBS for 7 min and treated with PBST for 10min to remove residual PFA. The slides were dehydrated by ethanol series (50%, 70%, 80%, 90%, 95%, and 100% x3) and preserved at -80℃ until use.

Immunohistochemistry

Testes from adult zebrafish were fixed in 4% PFA in PBS at 4℃ for overnight. Fixed testes were dehydrated by ethanol series (50%~100%), methyl benzoate and Lemosol (Wako). After dehydration, testes were embedded in paraffin, and sectioned at a thickness of 5 µm using rotary microtome. Sections were pasted onto FRONTIER-coated micro slide glasses (Matsunami Glass Ind Ltd., Osaka, Japan) and dried for overnight.

The slides were deparaffinized by xylene and rehydrated by ethanol series (100% x2, 90%, 80% and 70%) and water. After rehydration, antigen was retrieved by using Immuno-Savior (Nisshin EM, Japan) as manufacturer's protocol. And then slides were blocked in 10% fetal bovine serum (FBS) in PBS at RT for 1 hour. After blocking,

blocking solution was wiped out. The primary antibody was diluted with 10% FBS in PBS, and sections were treated by those solutions at 4℃ for overnight. After immunoreaction, slides were washed with PBS 3 times, and blocked by 10% FBS in PBS for an hour in RT. Blocking solution was wiped out and treated with the secondary antibody diluted by 10% FBS in PBS. The third antibody and fluorophore-conjugated streptavidin were used in same procedures as the secondary antibody. After the secondary, third antibody or fluorophore-conjugated streptavidin treatment, slides were counter-stained by DAPI and washed by PBS 2 times. Washed sections were mounted by VECTASHIELD (VECTOR) and observed in fluorescent microscope.

Antibodies were used at the following dilution: guinea pig anti-Sycp2C499 antibody (1:500), rabbit anti-Sycp3 antibody (1:500, (Ozaki et al., 2011), rat anti-Sycp1 antibody (1:500, (Saito et al., 2014)) , mouse anti-Sycp1 antibody (1:500, (Saito et al., 2014)) , goat anti-guinea pig IgG AP conjugated (1:500, SantaCruz), goat anti-guinea pig IgG alexa488 conjugated (1:500, Jackson Immunoreserch Laboratories) ,goat anti-guinea pig IgG biotin conjugated(1:500, Vector Laboratories), goat anti-rat IgG biotin conjugated (1:500, Vector Laboratories) goat anti-rabbit IgG Cy3 conjugated (1:500, Abcam), goat anti-rabbit IgG cruzfluore488 conjugated (1:500, SantaCruz), goat anti-rat IgG alexa 488 conjugated (1:500, Molecular probes), mouse monoclonal anti-biotin antibody Cy3 conjugated (1:500, SIGMA) and goat anti-mouse IgG alexa 594 conjugated (1:500, Molecular probes). Fluorophore conjugated avidin was used at following dilution; streptoavidin alexa 488 conjugated (1:500, Molecular probes)

Immunocytochemistry

Spread spermatocytes on MAS-coated slide were blocked by 5% FBS 5% Skim milk in PBS for 1 hour at room temperature. After blocking, blocking solution was wiped out and slides were treated by primary antibodies diluted in 5% FBS and 5 % skim milk in PBS at 4℃ for overnight. After antibody treatment, slides were washed with PBS for 5 mins trice and blocked by 5% FBS and 5% skim milk in PBS for 1 hour at room temperature. After that, blocking solution was wiped out and slides were treated by secondary antibodies diluted in 5% FBS and 5% skim milk in PBS at room temperature for 90 mins. Finally, slides were washed by PBS containing DAPI once and washed by PBS twice. Washed sections were mounted by VECTASHIELD (VECTOR) and observed in fluorescent microscope.

Fluorescent in situ hybridization (FISH) for telomere

Sections or spread spermatocytes treated with secondary antibodies conjugated with fluorophores were post-fixed by 1% PFA in PBS for 15 mins at room temperature. Slides were washed by PBS 3 times. Washed slides were treated by FISH buffer (20 mM Tris-HCl pH 6.8, 0.5% BSA, 70% deionized formamide) containing peptide nucleic acid (PNA) probe (Panagene) complement to telomere ($(CCCTAA)_3$) conjugated with Cy3 (0.2 μg/ml). Slides were first incubated in 80℃ for 9 mins and then incubated at 37℃ for 2 hours in dark condition in hybridization incubator HB-80 (TAITEC). After incubation, slides were washed by wash buffer (20 mM Tris-HCl pH 6.8, 70% deionized formamide) for 15 mins. Finally, slides were washed by PBS containing DAPI once and washed by PBS 2 times. Washed slides were mounted by VECTASHIELD (VECTOR) and observed in fluorescent microscope.

4. Results

Expression of *sycp2* is lower in the *its* mutant than in WT

The genes in a causal genomic region are shown in Table 1 (This mapping was performed by Dr. Saito). This region is located between SSLP markers z20895 and z7550. Among them, genes related to meiotic chromosome architecture were *sycp2* and *smc1al*. To examine the expression of these genes in testes, RT-qPCR was performed using primers set at 3' side of these genes (Fig. 3). Several reference genes were used to avoid bias by the different testes components between WT and the *its* mutant. Using *actb1* as reference, *sycp2* showed 70 % of reduction compared with WT and this was statistically significant while *smc1al* did not show any reduction (Fig. 3A). Using *rps29* as reference, *sycp2* also showed 70% of reduction compared with WT while *smc1al* did not show any reduction (Fig. 3B). To avoid the bias caused by different cellular composition of testes in the *its* mutant which show accumulation of Sycp3 positive spermatocytes (Saito et al., 2011), other spermatocyte-specific *sycp1* and *sycp3* were also used as references (Fig. 4). Expressions of *sycp1* and *sycp3* in the *its* mutant which shows accumulation of spermatocytes were not significantly different compared with those of WT (Fig. 4C, D). Using these reference, *sycp2* showed 60 % (Fig. 4A) and 90 % (Fig .4B) of reduction in the *its* mutant, and these reduction were statistically significant.

To confirm the reduction of *sycp2* mRNA in the *its* mutant, further RT-qPCR was performed using primers set in 5' side of *sycp2* mRNA (Fig. 13). Using these primer pair, the *its* mutant showed significantly lower expression of *sycp2* compared with WT (Fig. 13B, compare wt and *its*.).

Thus, in *its* homozygous mutant testes, the expression level of *sycp2*, a gene related to meiotic chromosome, was reduced, but *smc1al* was intact.

Homozygous KO of *sycp2* results in sterility in male

To check the phenotype of KO of *sycp2* and to use in complementation test with the *its* mutant, TALENs are designed against Exon18 (Fig. 5A). Because there are many ATG codons that can cause the translation of short truncated protein in 5' side of the *sycp2* mRNA, I chose this exon as a target of TALEN. By the injections of TALEN mRNAs into about 50 embryos at the 1-4 cells stage, 7 founder fishes were obtained after the screening of 9 injected fishes. From these fishes, one founder produced three lines of deletion mutants with, 14, 16 and 3 bp deletions respectively (Fig. 5B). Among these, the KO with 14 bp deletion was used as *sycp2* KO for further experiments. This KO showed drastic reduction of mRNA of *sycp2* (Fig.5D, E). The *its* mutant showed relatively higher expression compared with the KO, however, the difference was not statistically significant. No adult female fish was found in homozygous *sycp2* KO same as the *its* mutant in the report by Saito et al. (2011). Six male *sycp2* KO fishes were crossed with WT female, and could not fertilize the eggs (Table 2). No sperm was observed in testes of sycp2 KO (Fig. 5C). Thus, *sycp2* KO is sterile same as the *its* mutant.

***sycp2* KO does not complement the phenotype of the *its* mutant**

To perform complementation test, the *its* heterozygous mutant (*sycp2* $^{its/IM}$) female was crossed with heterozygous *sycp2* KO male (*sycp2* $^{KO/India}$) (Fig. 6). Scheme of genotyping for complementation tests is shown in Fig.6 A. From the offspring of

complementation test cross, heterozygous mutants at target sites of TALEN were first isolated (Fig. 6A, B, asterisks). Further, isolated heterozygous KO fish (*sycp2* $^{KO/IM}$ or *sycp2* $^{KO/its}$), were again genotyped by SSLP marker z20895 (Fig.6A, C, asterisks) and heterozygous fish at this marker were isolated. Finally, these fishes (*sycp2* $^{KO/its\ z20895}$) were again genotyped by another SSLP marker z7550 to check the absence of IM allele (Fig. 6A, D arrow). Finally, 17 fishes out of 67 offspring were revealed to be *sycp2*$^{KO/its}$ fish in the complementation test cross. This ratio coincided well with the 1/4 Mendelian ratio. Five *sycp2*$^{KO/its}$ fishes were crossed with WT female, and they could not fertilize the eggs (Table 3). These fishes had no sperm in testes same as *sycp2* KO and the *its* mutant, and had no phenotypic difference compared with *sycp2* KO or the *its* mutant by HE staining (Fig. 6E). Thus, *sycp2* KO did not complement the phenotype of the *its* mutant, indicating that the *its* mutant has defect in *sycp2* expression.

In the *its* mutant, synapsis from telomere bouquet is maintained

In the *its* mutant the expression of *sycp2* was thought to be defective. To check the any possible phenotypic difference of the *its* mutant and *sycp2* KO, immunohistochemistry against Sycp3 and Sycp1 was performed (Fig. 7). In WT, all stages of prophase I from preleptotene to pachytene identified by the localization pattern of Sycp3 and Sycp1 were detected as described in previous study (Saito et al., 2014). In *sycp2* KO, Sycp3 formed large aggregates in nuclei and Sycp1 formed short rod-shape SCs-like structures that did not co-localize with Sycp3 (Fig. 7; *sycp2* (-/-), inset). This phenotype resembles well that of mouse *Sycp2* KO (Yang et al., 2006). In the *its* mutant, Sycp3 formed large aggregates same as in *sycp2* KO. However, interestingly in the *its* mutant, Sycp1 formed WT-like SCs-like structure dispersed throughout nucleus like networks (Fig. 7;

its (-/-), left cyst). And some cysts showed synapsis from one pole of nuclei (Fig. 7; *its* (-/-), right cyst and inset). To check the morphology of these spermatocytes in detail, immunocytochemistry on spermatocytes spread was performed (Fig. 8). In WT, formation of AE/LEs and synapsis from one pole of nuclei was detected same as previous study (Saito et al., 2014). In *sycp2* KO, Sycp3 formed large aggregates in the nuclei and Sycp1 formed aberrant synapsis. In the *its* mutant, Sycp3 formed aggregates while synapsis shown by Sycp1 from one pole of nuclei was observed. To check whether this one pole of nuclei coincides with telomere bouquet like WT or not, combination staining by immunohistochemistry or -cytochemistry and telomere FISH was performed (Fig. 9). The *its* mutant testes showed co-localization of telomere bouquet and pole of Sycp1 formation as same as WT testes while *sycp2* KO did not show such structures. Thus, the synapsis was started from telomere bouquet in the *its* mutant.

Sycp2 protein in the *its* mutant testes was hardly detected

By immunostaining, the *its* mutant showed phenotypic difference with *sycp2* KO (Fig. 7, 8, 9). Then, the amount of Sycp2 expression in the *its* mutant testes is needed to be estimated by western blotting or immunoprecipitation (Fig. 10). To perform this experiment, Sycp2 C-terminal specific antibody was raised (Fig. 10A). This antibody specifically recognized Sycp2 (Fig. 10B; arrowhead, compare WT and KO). However, the *its* mutant did not show specific band. Immunoprecipitation of Sycp2 also could not detect the specific band in the *its* mutant while it was successfully concentrated in WT. To further check presence of Sycp2 protein in the *its* mutant, I also performed immunohistochemistry of Sycp2 and Sycp3 using WT, *sycp2* KO and the *its* mutant

testes (Fig. 11). In WT, spermatocytes in zygotene-pachytene showed co-localization of Sycp2 and Sycp3. However, both *sycp2* KO and the *its* mutant did not show Sycp2 signals in nucleus of any spermatocytes while most spermatocytes showed large aggregate of Sycp3. Thus, the amount of the Sycp2 protein in the *its* mutant should be extremely low.

Intron 3 which is minor intron that often retained in mRNA is not the cause of the *its* mutant

Although the previous study could not find any mutation in ORF of *sycp2* in the *its* mutant, *sycp2* KO could not complement the phenotype of the *its* mutant. To find the causal genomic region related to *sycp2* mRNA expression, RT-PCR and cDNA cloning was performed (Fig. 12, 13) because I could not find any mutation in 3'-UTR and 2000 bp of presumptive promoter area (Fig. 12A). RT-PCR targeted to exon1-3, 3-5 and 4-6 which contain small introns were performed (Fig. 12B, C). Among those fragments, only exon 3-5 from the *its* mutant showed additional 100 bp larger band (Fig. 12C). By cloning and sequencing of this larger fragment, it is revealed that this larger fragment retain intron 3 which is minor intron. However, no mutation was found in intron 3 of the *its* mutant (data not shown). To assess the frequency of retention of intron 3 in the *its* mutant and *sycp2* KO, RT-qPCR was performed using primer pairs to detect spliced form and retained form (Fig. 12 D, E F). The amount of spliced form was significantly lower in the *its* mutant and *sycp2* KO than WT while spliced form did not show any difference (Fig. 12 E,F). This indicates that the detection of intron 3 retained form in the *its* mutant was resulted from relative increase of retained form caused by the reduction of spliced form. This reduction of spliced form is thought to be caused by

nonsense-mediated decay (NMD) which occurs in pioneer round of translation against aberrant mRNA containing premature termination codon such as in *sycp2* KO.

The *its* mutant has an aberrant 3'-splice site in intron8 that causes lower expression of intact mRNA

Coincidentally, during the process to search the retention of intron 3 using fragments of *sycp2* including exon 1-9, the other *its* mutant-specific transcript was obtained (Fig. 13). From the *its* mutant, in addition to normal *sycp2* mRNA, aberrant mRNA containing 5 bp insertion in junction between exon 8 and exon 9 was found (Fig. 13A). This insertion (TTTAG) contains in-frame termination codon and coincides with 3' end of intron 8.Genomic sequence of the *its* mutant revealed that T to A substitution just 6 bp before the 3' end of intron 8 that can create the aberrant 3'-splice site was found in 15 individuals among 15 *its* mutants (Fig. 13B). To check the splicing state of intron 8 in the *its* mutant, by RT-PCR of the *its* mutant RNA and cloning, the ratio of normally spliced clones and 5 bp inserted clone was estimated (Fig. 13C, D, E).Normally spliced clones were only 10 % in the *its* mutant.

Aberrant 3'-splice site in intron 8 dominantly acts in WT background

As shown in above, the *its* mutant has aberrant 3'-splice site in intron 8. However, splicing requires variety of cis-acting elements. To elucidate if this aberrant splice site works independent of the *its* mutant background or not, Tg lines possessing minigenes comprising exon 8, intron 8, and exon 9 of WT (WT-E8-9) or the *its* mutant (*its*-E8-9) with EGFP reporter driven a ubiquitous promoter (EF1a) were generated in WT background (Fig. 14A, B). Both strain expressed EGFP because of the presence of

kozac sequence in front of EGFP translational initiation codon ATG (Fig. 14A). To check the splicing of mRNA from each Tg lines, RT-PCR from adult caudal fin that do not express *sycp2* was performed (Fig. 14C, D). From *its*-E8-9, the shifted band compared to the band of WT-E8-9 was detected like *sycp2* of the *its* mutant. These results indicate that the T to A substitution in intron 8 of the *its* mutant creates a dominant splice site to the normal 5bp downstream splice site even in the WT background.

Sycp3 first assembled as AE/LEs in leptotene which Sycp2 first appear

Sycp2 has a role to provide the link between Sycp3 and Sycp1 in rodent models (Winkel et al., 2009). Several reports also shows the localization pattern of Sycp2 in meiosis prophase I (Kouznetsova et al., 2011; Offenberg et al., 1998; Yang et al., 2006), however, the dynamics of Sycp2 along the process of meiosis prophase I is not yet determined. Thus, to assess the detail localization pattern of Sycp2 and its interaction dynamics with other SCs proteins in meiotic prophase I, I performed immunohistochemistry and immunocytochemistry of Sycp2 and Sycp3 or Sycp1 using WT testes (Fig. 15, 17). In preleptotene spermatocytes in which Sycp3 formed large aggregates, Sycp2 was not detected in nuclei (Fig. 15). After leptotene stage in which only Sycp2 (Fig. 15) and Sycp3 localize one pole of nuclei (Fig. 7), Sycp2 co-localized with Sycp3 (Fig. 15). In further stage, zygotene and pachytene, Sycp2 co-localized with both Sycp1 (Fig. 16) and Sycp3 (Fig. 15). Thus, Sycp2 showed different localization pattern from Sycp3 even though these are AE/LE proteins. From preleptotene Sycp3 appears first as aggregate in nuvlei, and then after Sycp2 appears, Sycp3 finally localizes to one pole of nuclei as AE/LEs.

5. Discussion

In this study, I observed the reduced amount of *sycp2* mRNA in the *its* mutant (Figs. 3, 4), and identified a single nucleotide substitution in the intron 8 of the *sycp2* gene in the *its* mutant. This substitution generates an aberrant 3'-splice site which causes insertion of 5 bp of residual intron 8 containing a premature termination codon (PTC) (Fig. 13). The transgenic experiment of minigene of this aberrant 3'splice site shows that the aberrant splice site acts more dominantly than the WT one independent of genetic background of the *its* mutant (Fig. 14). Severe defects of *sycp2* mRNA production were also observed in *sycp2* KO fish that is introduced PTC in the *sycp2* gene by deletion in the exon 18 (Fig. 5). Therefore, it is highly probable that the single nucleotide substitution is causative mutation of the *its* mutant. However, the present results are not able to deny the possibility that there is another mutation which causes the *its* phenotype. Sequencing of entire *sycp2* transcripts of the *its* mutant is currently under investigation. Interestingly, in the *its* mutant which critically reduces the expression of *sycp2*, the synapsis indicated by Sycp1 was initiated from telomere bouquet similarly to that of WT, while not in the KO which lack WT Sycp2 protein. Difference between the *its* mutant and KO is that small amounts of normal *sycp2* mRNA were detected in the *its* mutant but not in KO. Although the Sycp2 protein was not detected in the *its* mutant by immunohistochemistry and immunoprecipitation of Sycp2 from testes lysates, it is likely that small amount of Sycp2 protein exist in *its* mutant. Based on observations of SYCP2 KO in rodent and the case of this study, I interpret that the Sycp2 protein is crucial for connecting SCs to telomeres (Fig. 17). In following section, I discuss the significance of the role of Sycp2 and the phenotype of the *its* mutant.

Meiotic chromosome architecture and Sycp2

Sycp2 is an AE/LE protein well conserved in vertebrate-lineage (Fraune et al., 2014). Although the telomere localization of Sycp2 was reported (Liebe et al., 2006), however, it was difficult to assess the actual roles of Sycp2 at telomeres in rodent models because the AE/LE proteins in rodent models first disperse throughout nucleus in leptotene before they form distinguishable AEs (Fig. 1A) (Llano et al.,2012; de la Fuente et al., 2007; Judis et al., 2004) and the proportion of cells in the telomere bouquet stage is quite low (Liebe et al., 2006). On the other hand, among vertebrate models, zebrafish shows specific meiotic chromosome dynamics in which synapsis is initiated at the telomere bouquet stage (Fig. 1B) (Saito et al., 2014). Taking the advantage of specific meiotic chromosome dynamics of zebrafish and reduced amount of the *sycp2* expression in the *its* mutant, the role of Sycp2 protein at telomere is suggested (Fig. 17). Recently, an in vitro study showed that Sycp2 can interact with centromeric proteins (Feng et al., 2017). Taken together, Sycp2 may have functions to interact with chromosomal landmarks such as telomeres or centromeres. To assess the role of Sycp2 at centromere in vivo, it is attractive to use zebrafish as a model.

Interestingly, Sycp1 and Sycp3 showed drastically different localization in the *its* mutant and *sycp2* KO. Sycp1 showed connection to the telomere bouquet only in the *its* mutant but not in *sycp2* KO spermatocytes (Figs. 7, 8, 9 11). In contrast, the Sycp3 protein showed severe aggregation in the *its* mutant, *sycp2* KO zebrafish in this study and *Sycp2* KO mice in the previous study (Figs. 7, 8, 9) (Yang et al., 2006). To explain the reason why only the localization of Sycp1 was maintained in the *its* mutant while Sycp3 showed aggregation both in the *its* mutant and *sycp2* KO, it is thought that the

presence of the Sycp2 protein and the difference of self-assembly property of the Sycp1 protein and the Sycp3 protein. In preleptotene to leptotene, Sycp3 first appears as large aggregates not only in zebrafish but also in mammals (Figs. 7, 8, 9, 15) (Scherthan et al., 1996; Ishiguro et al., 2011; Saito et al., 2014). After leptotene when Sycp2 appears, Sycp3 forms thread-like structures (Figs. 7, 15, 16) with some aggregates. The lack or reduction of the Sycp2 protein in *sycp2* KO or in the *its* mutant zebrafish coincides with this transformation of Sycp3 aggregate into thread-like form (Figs. 15, 16). Yuan et al. (1998) showed that rat SCP3 can form fibers in COS-7 cells and 3T3 cells, however, those fibers are formed in cytoplasm, and electronmicroscopy revealed that the fiber-like structure in nucleus are not like SCs but like wool balls. Additionally, SCP3 in nucleus looked granular rather than fiber, and did not co-localize with rat SCP1 which was excluded from nucleus and only diffused in cytoplasm. However, they did not discuss the localization of SCP1 and SCP3 in nucleus. Furthermore, by co-expression of SCP2 and SCP3 in COS cells, both protein co-localize as more apparent fiber than the single expression of SCP3 (Pelttari et al., 2001). From these observations, it is suggested that the transformation of the Sycp3 protein from aggregate to the thread-like form requires the Sycp2 protein in nucleus. In case of the *its* mutant, a low amount of the Sycp2 protein could be expressed from intact *sycp2* mRNAs, and that protein level might be insufficient to prevent aggregation of Sycp3. To examine this idea in detail, further biochemical analysis will be required. On the other hand, Sycp1 tends to show a SC-like localization pattern even in the case of its cytoplasmic expression in COS-7 cells (Öllinger et al., 2005) and in the absence of both Sycp2 and Sycp3 in spermatocytes (Figs. 7, 8, 9) (Yuan et al., 2000; Yang et al., 2006). Furthermore, TF and CE proteins in yeast, fruit fly and worm which are functionally

same as vertebrate ones show strong self-assemble ability (Rog et al., 2017). In the *its* mutant, an extremely low amount of the Sycp2 protein could be translated. In addition, mammalian SYCP2 proteins are known to bridge SYCP1 and SYCP3 (Winkel et al., 2009). Furthermore, SYCP2 can localize onto telomeres without SYCP3 (Liebe et al., 2004). Therefore, the synapsis from the telomere bouquet is enabled by the strong self-assemble ability of the Sycp1 protein and CE proteins supported by the telomere localization of Sycp2 (Fig. 17). Although majority of the *sycp2* mRNA is degraded in the *its* mutant, there is the possibility that a small amount of an N-terminal truncated protein could be localized at telomeres (Fig. 17). However, Yang et al. (2006) showed the presence of an N-terminal truncated SYCP2 protein in their *Sycp2* KO mice in which the connection of SC-like structures to telomeres were not observed. Additionally, RT-qPCR in 5' side of *sycp2* showed statistically significant reduction of the *sycp2* mRNA expression (Fig. 12). Furthermore, *sycp2* KO zebrafish in this study also potentially expresses an N-terminal truncated protein (Fig. 10), however, *sycp2* KO zebrafish did not show connection of SC-like structure indicated by Sycp1 and telomeres (Figs. 7, 8, 9). Thus, the effect of truncation of the Sycp2 protein in the *its* mutant would be small even if it is expressed. Taken together, it is suggested that the Sycp2 protein is the connector protein of SCs to telomeres while it is an AE/LE protein.

SCs formation from the telomere bouquet in teleosts

The ability of the Sycp2 protein to localize on telomeres could be conserved in vertebrates from as shown above. In the cytoplasmic locus adjacent to where the bouquet exists, centrosomes marked by γ-tubulin are detected both in rodents and teleosts (Saito et al., 2014; Tomita and Cooper, 2006). While this property around the

bouquet is conserved between mammals and teleosts, meiotic chromosome dynamics show drastic difference among these vertebrates. The AE/LEs of mammalian meiotic chromosomes begin to be formed throughout the nucleus along the chromosomes. Synapsis starts after the formation of AE/LEs (Stanzione et al., 2016). On the other hand, in teleost, both AE/LE formation and synapsis initiated from one pole of nucleus where the telomere bouquet exists (Saito et al., 2014; Iwai et al., 2006) (Fig. 1B). There is no information about the cause of teleosts-specific elongating formation of SCs, however, cytological difference coincides well with this SC formation exists in nuclear membrane. In nuclear membrane of rodents spermatocytes, the telomere bouquet is formed in the locus without nuclear pore complex (NPC) in a mutual exclusive manner (Scherthan et al., 2000). In contrast, zebrafish oocytes show co-localization of the telomere bouquet and NPCs (Elkouby et al., 2016). This difference between zebrafish and rodents in localizations of NPCs might cause the difference of SCs formation in vertebrates. To unveil primary mechanisms that support elongating SCs formation from the telomere bouquet, other experimental approaches like meiosis-specific conditional KO of NPCs are required. Nevertheless, my study showed that a small amount of the Sycp2 protein expressed translated from a small amount of WT *sycp2* mRNA in the *its* mutant appeared to be sufficient for the connection of SCs to the telomere bouquet (Figs. 7, 8, 9, 12, 16).

Reduction of mRNA of *sycp2* transcripts in the *its* mutant.

RT-qPCR analysis of the *its* mutant showed about 80% of reduction of the *sycp2* mRNA in homozygous testes, while fertile heterozygous testes showed about 50% of reduction compared with WT testes (Figs. 3, 4). This reduction can be explained by

nonsense mediated decay (NMD) (Ishigaki et al., 2001) that is triggered by PTCs. NMD is well studied mechanisms controlling quality of mRNAs. NMD requires the exon junction complex (EJCs) which is deposited close to exon junctions (Kashima et al., 2006). By EJCs and ribosome running in the pioneer round of translation, PTC downstream of exon junction is recognized and decayed in the pioneer round of translation (Ishigaki et al., 2001; Kashima et al., 2006). In all RT-(q)PCR experiments in this study, I used oligo-dT primer for reverse-transcription to obtain cDNAs of mature mRNA and primers for were set to 3' sides of ORFs for qPCR to avoid bias of reverse transcription caused by RNA degeneration. In the *its* homozygous mutant, *sycp2* transcripts contain both the normal mRNA and abnormal one containing a 5 bp insertion with PTC. The ratio of the abnormal mRNA reached to 90 % (Fig. 13). This ratio coincides well with the result of RT-qPCR (Figs. 3, 4). Here the *its* mutant showed reduction of the *sycp2* mRNA reaching to 80 %. Thus, the consistency of these results supports by the idea that the mRNAs generated by mis-splicing of intron 8 in the *its* mutant is targeted by NMD. Furthermore, the minigene containing a genomic locus spanning exon 8 to exon 9 of *sycp2* from the *its* mutant showed insertion of 5 bp residual intron 8 even in the WT background (Fig. 14). Both the WT and the *its* mutant minigenes expressed EGFP because of the lack of the Kozak sequence before ATG of *sycp2* exon 8 in these minigenes. NMD occurs in the pioneer round of translation (Ishigaki et al., 2001). Both minigenes are actually transcribed and spliced (Fig. 14). However, before the first ATG, there is no Kozak sequence. Thus, ribosomes cannot recognize the *sycp2* locus of mRNA from the minigenes. Then ribosome only starts translation from the EGFP locus and do not start translation from the *sycp2* locus in the minigene. Thus, ribosome in the pioneer round cannot recognize PTC resulting from

mis-splicing caused by the *its* mutation. Finally, NMD does not occur in the minigene with the *its* mutation. Although there is a possibility of the presence of another mutation in the *sycp2* genomic locus of the *its* mutant, however, the reduction of *sycp2* mRNA is more likely to be the result of the mutation in intron 8.

Mis-splicing by the *its* mutation in *sycp2* intron 8

In the *its* mutant, T to A substitution in intron 8 of *sycp2* resulted in an aberrant 3'-splice site which causes mis-splicing in 90 % of its transcripts (Fig. 13). This mis-splicing is not due to trans-acting factors in the mutant background because the minigene containing intron 8 from the *its* mutant also showed mis-splicing in the WT background. The reason why this mutation causes strong bias for mis-splicing is unknown. The simple answer for this question could be change in affinity of the 3'-splice site and spliceosome (Sohail and Xie, 2015). In the *its* mutant, by the aberrant 3'-splice site, the region around there could be recognized as a strong splice site. In case of human with infertility, not only mutations of meiotic genes in exons but also in introns are often reported (Yang et al., 2015). However, in model vertebrate organisms, sterile mutant lines caused by intronic mutation is hard to find and difficult to generate by targeted mutagenesis because of lack of detail knowledge about splicing regulators in genomic sequences (Kuroyanagi et al., 2013). To my knowledge, the *its* mutant is the first case of mutant carrying mutation in intron that shows infertility, less gene expression levels and different meiotic chromosome architecture from KO of same gene in vertebrate model. Recently, Yoshida et al. (2015) reported that not complete, but drastic increase of exon 20 skipping in the IKBKAP gene in neuronal tissue which causes familial dysautonomia (FD) could be treated by a small molecule which is a drug

candidate, rectifier of aberrant splicing (RECTAS). This exon skipping is caused by change in the affinity between spliceosome and 5'-splice sites due to the T to C substitution of the 6th nucleotide of intron 20 of the IKBKAP gene. In that study, authors used a cell culture system containing both normal and patient type of the minigenes to determine the effects of small molecules. After the finding of spliceostatin A (Kaida et al., 2007), medical genomics related to splicing defects via drug development increase its social importance. However, these studies based only on in vitro or cultured cell systems. To assure therapeutic effects of small molecules as drug candidates, in vivo models are required. Although the causal intronic mutation of exon skipping in FD is different from that of mis-splicing of the *its* mutant, causal mechanisms of both mis-splicing events can be explained by change in affinity between spliceosome and splice sites. Therefore, the *its* mutant could be used as a clinical model animal especially in screening of the drug candidate to cure the splicing defect and also in the basic study of splicing such as the occurrence of alternative 3' splice site(Koren et al., 2007) .

As shown in above, by my analysis of the *its* mutant, several insights into vertebrate meiosis have been suggested 1) in teleost, the synapsis initiates at telomere with the supported by telomere localization of the Sycp2 protein, 2) the role of Sycp2 at telomere is conserved in vertebrates, 3) the mutation in intron of the meiotic genes cause aberrant splicing resulting into meiotic arrest and sterility. To demonstrate the cause of the *its* mutant and the role of Sycp2 at telomere, further sequencing analysis and biochemical analysis are required. However, this study provides the distinct foothold to understand the meiotic chromosome architecture and the expression regulation of meiotic genes.

6. Conclusion

This study shows that the *its* mutant is a hypomorphic mutant of *sycp2* caused by the formation of an aberrant 3'-splice site in intron 8 that cause mis-splicing resulting in occurrence of PTC in most of mRNA of *sycp2*. This is the first report of intronic mutant in vertebrate model clearly related to male infertility and meiotic chromosome architecture. By the analysis of the phenotype of the *its* mutant and *sycp2* KO, I also showed that Sycp2 protein was a connector protein of SCs to telomeres that is distinct from any other SCs proteins. Taken together, it is suggested that the correct meiotic chromosome architecture is achieved not by just a presence of the component genes, but by sufficient amount of those expressions.

7. Acknowledgements

Here, I express my gratitude to all members for providing me advice, technical help, daily encouragement during the preparation of this study.

First of all, I am grateful to Assoc. Prof. Noriyoshi Sakai for his preserving and critical suggestion, encouragement for this Ph.D. thesis. I thank all progress committee members: Drs. Yumiko Saga, Hiroyuki Araki, Masato Kanemaki and Ken-ichi Nonomura for good discussions and advice from the time of my entrance to SOKENDAI. I also thank all members of Model Fish Genomics Resource Laboratory, Dr. Toshihiro Kawasaki and Dr. Yukiko Imai for daily and deep discussion and great technical advice in daily experiments and Ms. Ayako Otake, Yasuko Kida, Yukiko Yoshida for daily care of fish used in this study and support of routine experiment. I greatly appreciate Assoc. Prof. Keiichiro Ishiguro for stimulating my motivation through discussion; Dr. Kenji Saito for the initial study including mapping requires hard work; Prof. Koichi Kawakami for providing pT2A-L200R150G vectors.

8. References

Bannister, L.A., Reinholdt, L.G., Munroe, R.J., and Schimenti, J.C. (2004). Positional cloning and characterization of mousemei8, a disrupted allele of the meiotic cohesinRec8. Genesis *40*, 184–194.

Bolcun-Filas, E., Speed, R., Taggart, M., Grey, C., de Massy, B., Benavente, R., and Cooke, H.J. (2009). Mutation of the Mouse Syce1 Gene Disrupts Synapsis and Suggests a Link between Synaptonemal Complex Structural Components and DNA Repair. PLoS Genetics *5*, e1000393.

Bolor, H., Mori, T., Nishiyama, S., Ito, Y., Hosoba, E., Inagaki, H., Kogo, H., Ohye, T., Tsutsumi, M., Kato, T., et al. (2009). Mutations of the SYCP3 Gene in Women with Recurrent Pregnancy Loss. The American Journal of Human Genetics *84*, 14–20.

Brown, P.W., Judis, L., Chan, E.R., Schwartz, S., Seftel, A., Thomas, A., and Hassold, T.J. (2005). Meiotic Synapsis Proceeds from a Limited Number of Subtelomeric Sites in the Human Male. The American Journal of Human Genetics *77*, 556–566.

Cahoon, C.K., and Hawley, R.S. (2016). Regulating the construction and demolition of the synaptonemal complex. Nature Structural & Molecular Biology *23*, 369–377.

Cahoon, C.K., Yu, Z., Wang, Y., Guo, F., Unruh, J.R., Slaughter, B.D., and Hawley, R.S. (2017). Superresolution expansion microscopy reveals the three-dimensional organization of the *Drosophila* synaptonemal complex. Proceedings of the National Academy of Sciences *114*, E6857–E6866.

Cermak, T., Doyle, E.L., Christian, M., Wang, L., Zhang, Y., Schmidt, C., Baller, J.A., Somia, N.V., Bogdanove, A.J., and Voytas, D.F. (2011). Efficient design and assembly of custom TALEN and other TAL effector-based constructs for DNA targeting. Nucleic Acids Res. *39*, e82.

Chikashige, Y., Ding, D.Q., Funabiki, H., Haraguchi, T., Mashiko, S., Yanagida, M., and Hiraoka, Y. (1994). Telomere-led premeiotic chromosome movement in fission yeast. Science *264*, 270–273.

Doyle, E.L., Booher, N.J., Standage, D.S., Voytas, D.F., Brendel, V.P., VanDyk, J.K., and Bogdanove, A.J. (2012). TAL Effector-Nucleotide Targeter (TALE-NT) 2.0: tools for TAL effector design and target prediction. Nucleic Acids Res *40*, W117–W122.

Elkouby, Y.M., Jamieson-Lucy, A., and Mullins, M.C. (2016). Oocyte Polarization Is Coupled to the Chromosomal Bouquet, a Conserved Polarized Nuclear Configuration in Meiosis. PLOS Biology *14*, e1002335.

Feng, J., Fu, S., Cao, X., Wu, H., Lu, J., Zeng, M., Liu, L., Yang, X., and Shen, Y. (2017). Synaptonemal complex protein 2 (SYCP2) mediates the association of the centromere with the synaptonemal complex. Protein & Cell *8*, 538–543.

Fraune, J., Schramm, S., Alsheimer, M., and Benavente, R. (2012). The mammalian synaptonemal complex: Protein components, assembly and role in meiotic recombination. Experimental Cell Research *318*, 1340–1346.

Fraune, J., Brochier-Armanet, C., Alsheimer, M., Volff, J.-N., Schücker, K., and Benavente, R. (2016). Evolutionary history of the mammalian synaptonemal complex. Chromosoma *125*, 355–360.

de la Fuente, R., Parra, M.T., Viera, A., Calvente, A., Gómez, R., Suja, J.Á., Rufas, J.S., and Page, J. (2007). Meiotic Pairing and Segregation of Achiasmate Sex Chromosomes in Eutherian Mammals: The Role of SYCP3 Protein. PLoS Genetics *3*, e198.

Gómez-H, L., Felipe-Medina, N., Sánchez-Martín, M., Davies, O.R., Ramos, I., García-Tuñón, I., Rooij, D.G. de, Dereli, I., Tóth, A., Barbero, J.L., et al. (2016). C14ORF39/SIX6OS1 is a constituent of the synaptonemal complex and is essential for mouse fertility. Nature Communications *7*, ncomms13298.

Gruhn, J.R., Al-Asmar, N., Fasnacht, R., Maylor-Hagen, H., Peinado, V., Rubio, C., Broman, K.W., Hunt, P.A., and Hassold, T. (2016). Correlations between Synaptic Initiation and Meiotic Recombination: A Study of Humans and Mice. Am J Hum Genet *98*, 102–115.

Hawley, R.S. (2011). Solving a Meiotic LEGO ® Puzzle: Transverse Filaments and the Assembly of the Synaptonemal Complex in *Caenorhabditis elegans* : Figure 1. Genetics *189*, 405–409.

Ishigaki, Y., Li, X., Serin, G., and Maquat, L.E. (2001). Evidence for a Pioneer Round of mRNA Translation: mRNAs Subject to Nonsense-Mediated Decay in Mammalian Cells Are Bound by CBP80 and CBP20. Cell *106*, 607–617.

Ishiguro, K., Kim, J., Fujiyama‐Nakamura, S., Kato, S., and Watanabe, Y. (2011). A new meiosis‐specific cohesin complex implicated in the cohesin code for homologous pairing. EMBO Reports *12*, 267–275.

Iwai, T., Yoshii, A., Yokota, T., Sakai, C., Hori, H., Kanamori, A., and Yamashita, M. (2006a). Structural components of the synaptonemal complex, SYCP1 and SYCP3, in the medaka fish Oryzias latipes. Experimental Cell Research *312*, 2528–2537.

Iwai, T., Yoshii, A., Yokota, T., Sakai, C., Hori, H., Kanamori, A., and Yamashita, M. (2006b). Structural components of the synaptonemal complex, SYCP1 and SYCP3, in the medaka fish Oryzias latipes. Experimental Cell Research *312*, 2528–2537.

Judis, L., Chan, E.R., Schwartz, S., Seftel, A., and Hassold, T. (2004). Meiosis I arrest and azoospermia in an infertile male explained by failure of formation of a component of the synaptonemal complex. Fertility and Sterility *81*, 205–209.

Kaida, D., Motoyoshi, H., Tashiro, E., Nojima, T., Hagiwara, M., Ishigami, K., Watanabe, H., Kitahara, T., Yoshida, T., Nakajima, H., et al. (2007). Spliceostatin A targets SF3b and inhibits both splicing and nuclear retention of pre-mRNA. Nature Chemical Biology *3*, nchembio.2007.18.

Kashima, I., Yamashita, A., Izumi, N., Kataoka, N., Morishita, R., Hoshino, S., Ohno, M., Dreyfuss, G., and Ohno, S. (2006). Binding of a novel SMG-1–Upf1–eRF1–eRF3 complex (SURF) to the exon junction complex triggers Upf1 phosphorylation and nonsense-mediated mRNA decay. Genes Dev. *20*, 355–367.

Kawakami, K., Takeda, H., Kawakami, N., Kobayashi, M., Matsuda, N., and Mishina, M. (2004). A Transposon-Mediated Gene Trap Approach Identifies Developmentally Regulated Genes in Zebrafish. Developmental Cell *7*, 133–144.

Koren, E., Lev-Maor, G., and Ast, G. (2007). The Emergence of Alternative 3′ and 5′ Splice Site Exons from Constitutive Exons. PLOS Computational Biology *3*, e95.

Kouznetsova, A., Benavente, R., Pastink, A., and Höög, C. (2011). Meiosis in mice without a synaptonemal complex. PLoS One *6*, e28255.

Kuroyanagi, H., Watanabe, Y., and Hagiwara, M. (2013). CELF Family RNA–Binding Protein UNC-75 Regulates Two Sets of Mutually Exclusive Exons of the unc-32 Gene in Neuron-Specific Manners in Caenorhabditis elegans. PLoS Genetics *9*, e1003337.

Laemmli, U.K., Beguin, F., and Gujer-Kellenberger, G. (1970). A factor preventing the major head protein of bacteriophage T4 from random aggregation. J. Mol. Biol. *47*, 69–85.

Liebe, B., Alsheimer, M., Höög, C., Benavente, R., and Scherthan, H. (2004). Telomere Attachment, Meiotic Chromosome Condensation, Pairing, and Bouquet Stage Duration Are Modified in Spermatocytes Lacking Axial Elements. Mol. Biol. Cell *15*, 827–837.

Liebe, B., Petukhova, G., Barchi, M., Bellani, M., Braselmann, H., Nakano, T., Pandita, T.K., Jasin, M., Fornace, A., Meistrich, M.L., et al. (2006). Mutations that affect meiosis in male mice influence the dynamics of the mid-preleptotene and bouquet stages. Experimental Cell Research *312*, 3768–3781.

Llano, E., Herrán, Y., García-Tuñón, I., Gutiérrez-Caballero, C., de Álava, E., Barbero, J.L., Schimenti, J., de Rooij, D.G., Sánchez-Martín, M., and Pendás, A.M. (2012). Meiotic cohesin complexes are essential for the formation of the axial element in mice. The Journal of Cell Biology *197*, 877–885.

Lui, D.Y., and Colaiácovo, M.P. (2013). Meiotic Development in Caenorhabditis elegans. In Germ Cell Development in C. Elegans, T. Schedl, ed. (New York, NY: Springer New York), pp. 133–170.

Meuwissen, R.L., Offenberg, H.H., Dietrich, A.J., Riesewijk, A., van Iersel, M., and Heyting, C. (1992). A coiled-coil related protein specific for synapsed regions of meiotic prophase chromosomes. The EMBO Journal *11*, 5091.

Offenberg, H.H., Schalk, J.A., Meuwissen, R.L., van Aalderen, M., Kester, H.A., Dietrich, A.J., and Heyting, C. (1998). SCP2: a major protein component of the axial elements of synaptonemal complexes of the rat. Nucleic Acids Research *26*, 2572–2579.

Öllinger, R., Alsheimer, M., and Benavente, R. (2005). Mammalian Protein SCP1 Forms Synaptonemal Complex-like Structures in the Absence of Meiotic Chromosomes. Mol. Biol. Cell *16*, 212–217.

Ozaki, Y., Saito, K., Shinya, M., Kawasaki, T., and Sakai, N. (2011). Evaluation of Sycp3, Plzf and Cyclin B3 expression and suitability as spermatogonia and spermatocyte markers in zebrafish. Gene Expression Patterns *11*, 309–315.

Pelttari, J., Hoja, M.-R., Yuan, L., Liu, J.-G., Brundell, E., Moens, P., Santucci-Darmanin, S., Jessberger, R., Barbero, J.L., Heyting, C., et al. (2001). A Meiotic Chromosomal Core Consisting of Cohesin Complex Proteins Recruits DNA Recombination Proteins and Promotes Synapsis in the Absence of an Axial Element in Mammalian Meiotic Cells. Molecular and Cellular Biology *21*, 5667–5677.

Revenkova, E., Eijpe, M., Heyting, C., Hodges, C.A., Hunt, P.A., Liebe, B., Scherthan, H., and Jessberger, R. (2004). Cohesin SMC1β is required for meiotic chromosome dynamics, sister chromatid cohesion and DNA recombination. Nature Cell Biology *6*, 555–562.

Rog, O., Köhler, S., and Dernburg, A.F. (2017). The synaptonemal complex has liquid crystalline properties and spatially regulates meiotic recombination factors. Elife *6*, e21455.

RONG, M., MATSUDA, A., HIRAOKA, Y., and LEE, J. (2016). Meiotic cohesin subunits RAD21L and REC8 are positioned at distinct regions between lateral elements and transverse filaments in the synaptonemal complex of mouse spermatocytes. J Reprod Dev *62*, 623–630.

Saito, K., Siegfried, K.R., Nüsslein-Volhard, C., and Sakai, N. (2011). Isolation and cytogenetic characterization of zebrafish meiotic prophase I mutants. Developmental Dynamics *240*, 1779–1792.

Saito, K., Sakai, C., Kawasaki, T., and Sakai, N. (2014). Telomere distribution pattern and synapsis initiation during spermatogenesis in zebrafish: Telomere Behavior in Zebrafish Spermatocytes. Developmental Dynamics *243*, 1448–1456.

Sakuma, T., Hosoi, S., Woltjen, K., Suzuki, K., Kashiwagi, K., Wada, H., Ochiai, H., Miyamoto, T., Kawai, N., Sasakura, Y., et al. (2013). Efficient TALEN construction and evaluation methods for human cell and animal applications. Genes Cells *18*, 315–326.

Scherthan, H., Weich, S., Schwegler, H., Heyting, C., Härle, M., and Cremer, T. (1996). Centromere and telomere movements during early meiotic prophase of mouse and man are associated with the onset of chromosome pairing. The Journal of Cell Biology *134*, 1109–1125.

Scherthan, H., Jerratsch, M., Li, B., Smith, S., Hultén, M., Lock, T., and de Lange, T. (2000). Mammalian meiotic telomeres: protein composition and redistribution in relation to nuclear pores. Molecular Biology of the Cell *11*, 4189–4203.

Shibuya, H., and Watanabe, Y. (2014). The meiosis-specific modification of mammalian telomeres. Cell Cycle *13*, 2024–2028.

Shibuya, H., Hernández-Hernández, A., Morimoto, A., Negishi, L., Höög, C., and Watanabe, Y. (2015). MAJIN Links Telomeric DNA to the Nuclear Membrane by Exchanging Telomere Cap. Cell *163*, 1252–1266.

Shinya, M., and Sakai, N. (2011). Generation of Highly Homogeneous Strains of Zebrafish Through Full Sib-Pair Mating. G3: Genes, Genomes, Genetics *1*, 377–386.

Sohail, M., and Xie, J. (2015). Diverse regulation of 3′ splice site usage. Cell. Mol. Life Sci. *72*, 4771–4793.

Stanzione, M., Baumann, M., Papanikos, F., Dereli, I., Lange, J., Ramlal, A., Tränkner, D., Shibuya, H., de Massy, B., Watanabe, Y., et al. (2016). Meiotic DNA break formation requires the unsynapsed chromosome axis-binding protein IHO1 (CCDC36) in mice. Nature Cell Biology *18*, 1208–1220.

Tomita, K., and Cooper, J.P. (2006). The Meiotic Chromosomal Bouquet: SUN Collects Flowers. Cell *125*, 19–21.

Urasaki, A., Morvan, G., and Kawakami, K. (2006). Functional Dissection of the Tol2 Transposable Element Identified the Minimal cis-Sequence and a Highly Repetitive Sequence in the Subterminal Region Essential for Transposition. Genetics *174*, 639–649.

Winkel, K., Alsheimer, M., Öllinger, R., and Benavente, R. (2009). Protein SYCP2 provides a link between transverse filaments and lateral elements of mammalian synaptonemal complexes. Chromosoma *118*, 259–267.

Woglar, A., and Jantsch, V. (2014). Chromosome movement in meiosis I prophase of Caenorhabditis elegans. Chromosoma *123*, 15–24.

Xu, H., Beasley, M.D., Warren, W.D., van der Horst, G.T.J., and McKay, M.J. (2005). Absence of Mouse REC8 Cohesin Promotes Synapsis of Sister Chromatids in Meiosis. Developmental Cell *8*, 949–961.

Yang, F., Fuente, R.D.L., Leu, N.A., Baumann, C., McLaughlin, K.J., and Wang, P.J. (2006). Mouse SYCP2 is required for synaptonemal complex assembly and chromosomal synapsis during male meiosis. The Journal of Cell Biology *173*, 497–507.

Yang, F., Silber, S., Leu, N.A., Oates, R.D., Marszalek, J.D., Skaletsky, H., Brown, L.G., Rozen, S., Page, D.C., and Wang, P.J. (2015). TEX11 is mutated in infertile men with azoospermia and regulates genome-wide recombination rates in mouse. EMBO Molecular Medicine *7*, 1198–1210.

Yoshida, M., Kataoka, N., Miyauchi, K., Ohe, K., Iida, K., Yoshida, S., Nojima, T., Okuno, Y., Onogi, H., Usui, T., et al. (2015). Rectifier of aberrant mRNA splicing recovers tRNA modification in familial dysautonomia. PNAS *112*, 2764–2769.

Yuan, L., Pelttari, J., Brundell, E., Björkroth, B., Zhao, J., Liu, J.-G., Brismar, H., Daneholt, B., and Höög, C. (1998). The synaptonemal complex protein SCP3 can form multistranded, cross-striated fibers in vivo. The Journal of Cell Biology *142*, 331–339.

Yuan, L., Liu, J.-G., Zhao, J., Brundell, E., Daneholt, B., and Höög, C. (2000). The murine SCP3 gene is required for synaptonemal complex assembly, chromosome synapsis, and male fertility. Molecular Cell *5*, 73–83.

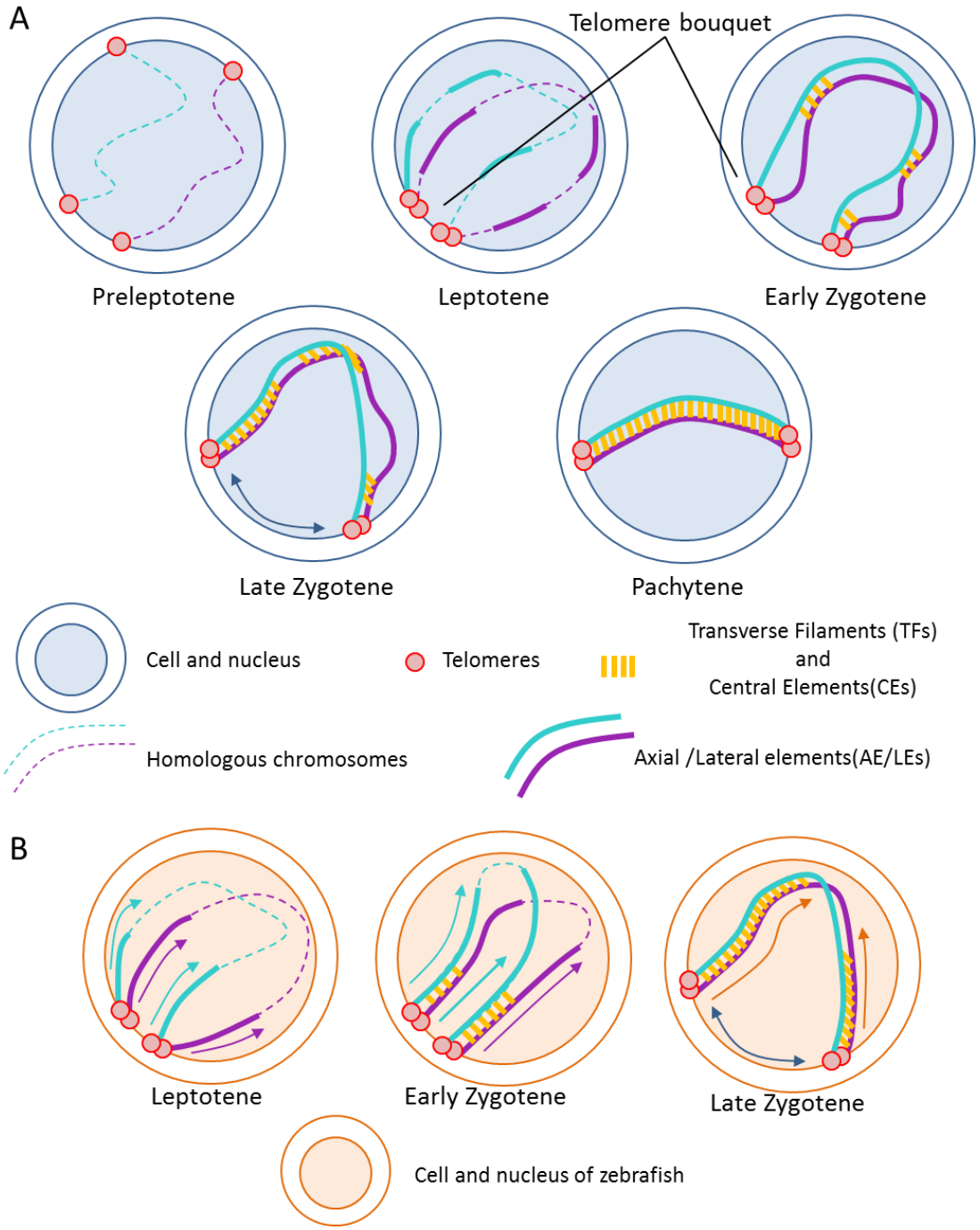

Figure 1. Mammalian model and zebrafish model of SCs formation. (A) General model of SCs formation. Telomeres attach to INM in preleptotene. AE/LE formation spread throughout nucleus and telomere bouquet is formed in leptotene. Homologous chromosomes synapse each other by TFs/CEs in early zygotene. Telomere bouquet are dispersed in late zygotene. Synapsis complete in pachytene. **(B)** Zebrafish model of SCs formation. AE/LEs are formed from telomere bouquet in leptotene. Synapsis of homologous chromosomes starts from telomere bouquet in zygotene.

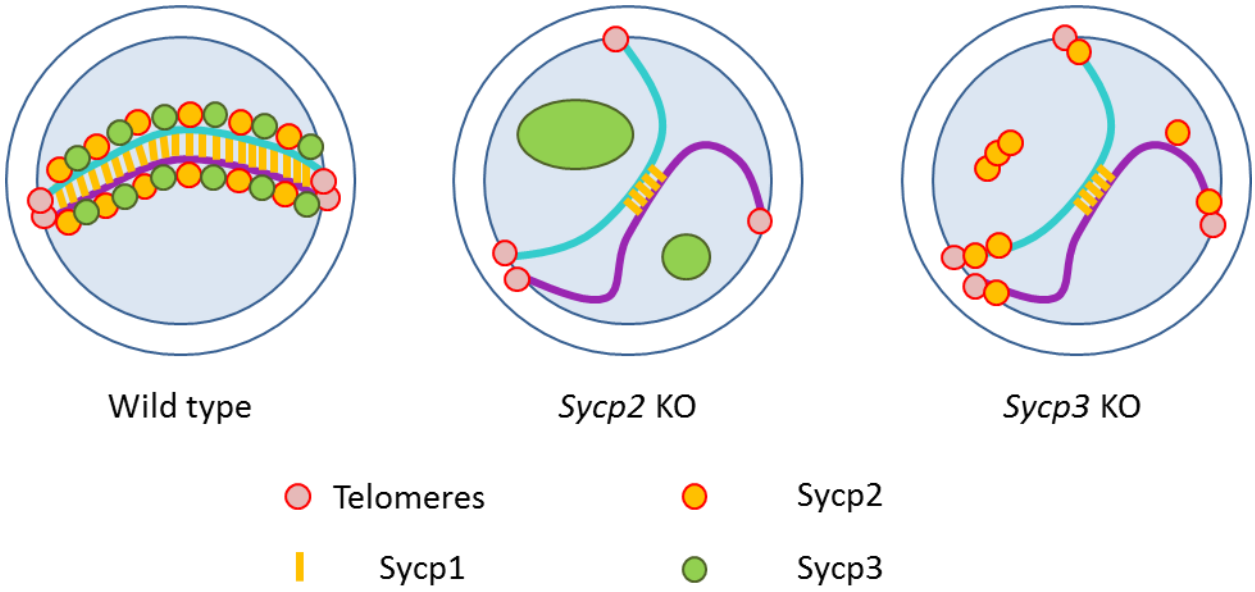

Figure 2. Phenotypes of AE/LEs mutants in rodent models. Wild type shows co-localization of Sycp2 and Sycp3 on chromosome axis as AE/LEs. In Sycp2 KO, SYCP3 form large aggregates in nucleus while SYCP1 form SCs-like structure. In Sycp3 KO, SYCP2 form small foci and thread-like structure that co-localize with telomeres while SYCP1 form SCs-like structure.

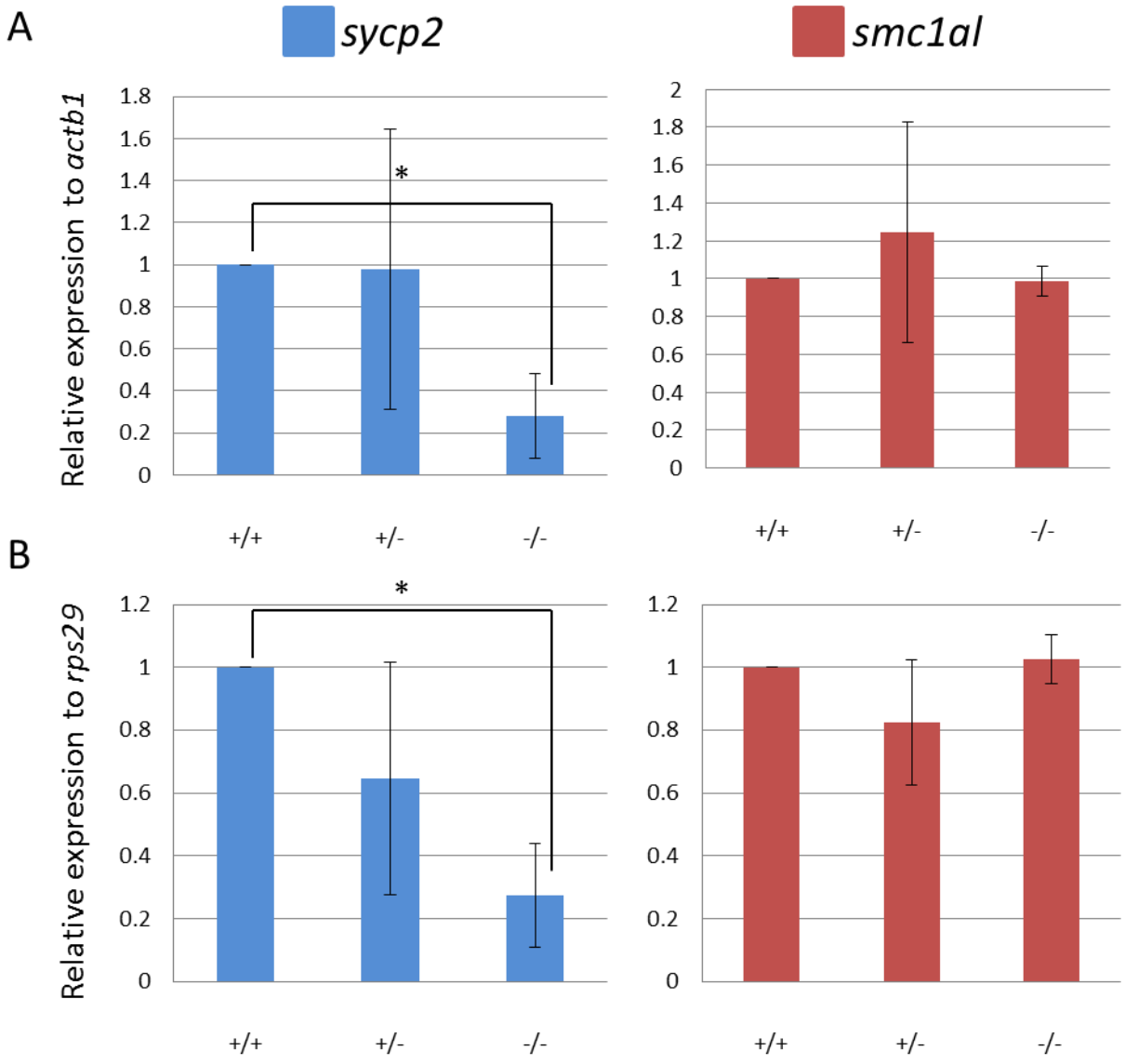

Figure 3. Expression of *sycp2* is lower in *its* mutant than WT while *smc1al* is same as WT. The expression level of *sycp2* and *smc1al* were estimated by RT-qPCR. **(A,B)** Expression level of *sycp2* and *smc1al* relative to *actb1*(A), and *rps29* (B). In both case, *its* homozygous mutant (-/-) showed statistically significant reduction compared with WT sibling (+/+) while *smc1al* did not show significant difference (n=3). Values represent the mean ±SD. *P<0.05

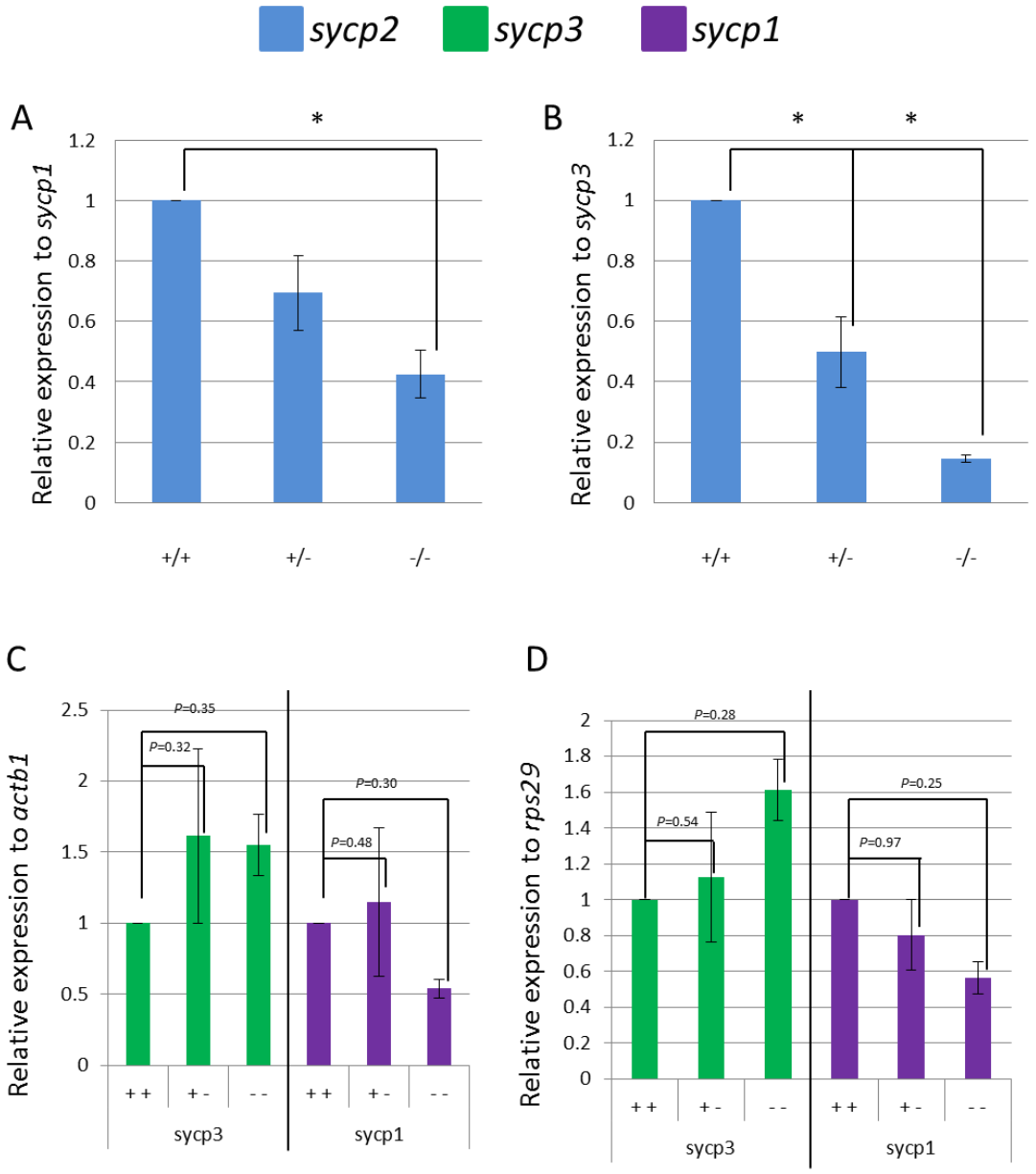

Figure 4. In *its* mutant, the amount of *sycp2* mRNA relative to *sycp1* and *sycp3* was reduced. (A,B) Expression level of *sycp2* relative to *sycp1* (A) and *sycp3* (B). In both case, *its* homozygous mutant showed statistically significant reduction compared with WT sibling (+/+) (n=3). **(C,D)** Expression levels of *sycp3* and *sycp1* relative to *actb1* (A) or *rps29* (B). In both case, *its* homozygous mutant did not show significant difference compared with WT sibling (++) or heterozygous mutant(+-) (n=3).Values represent the mean ±SD. *P<0.05

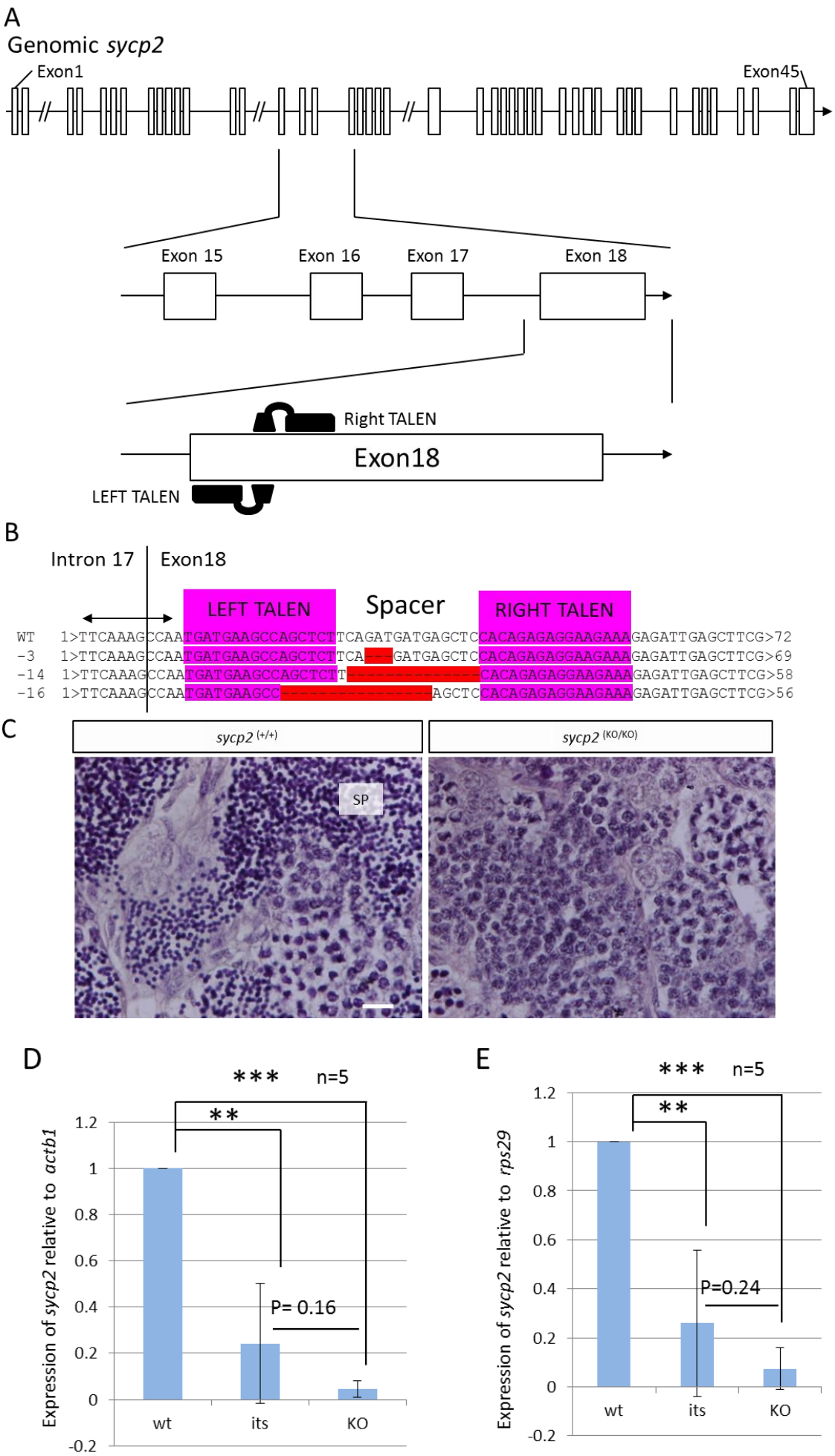
A
Genomic sycp2
Exon1
Exon45
Exon 15
Exon 16
Exon 17
Exon 18
Right TALEN
Exon18
LEFT TALEN
B
Intron 17
Exon18
LEFT TALEN
Spacer
RIGHT TALEN
WT 1>TTCAAAGCCAATGATGAAGCCAGCTCTTCAGATGATGAGCTCCACAGAGAGGAAGAAAGAGATTGAGCTTCG>72
-3 1>TTCAAAGCCAATGATGAAGCCAGCTCTTCA---GATGAGCTCCACAGAGAGGAAGAAAGAGATTGAGCTTCG>69
-14 1>TTCAAAGCCAATGATGAAGCCAGCTCTT----------CACAGAGAGGAAGAAAGAGATTGAGCTTCG>58
-16 1>TTCAAAGCCAATGATGAAGCC----------AGCTCCACAGAGAGGAAGAAAGAGATTGAGCTTCG>56
C
sycp2 (+/+)
sycp2 (KO/KO)
SP
D
***
n=5
**
P= 0.16
Expression of sycp2 relative to actb1
1.2
1
0.8
0.6
0.4
0.2
0
-0.2
wt
its
KO
E
***
n=5
**
P=0.24
Expression of sycp2 relative to rps29
1.2
1
0.8
0.6
0.4
0.2
0
-0.2
wt
its
KO

Figure 5. KO of *sycp2* by TALEN showed sterility same as mammalian model. (A) A schematic of genomic locus of *sycp2* gene and position of designed TALENs. The length from first ATG to termination codon in exon45 is about 60 kbp. Each blank box indicate exons. Long introns were omitted by double slash. **(B)** Detail design of TALENs in exon18 and resulting sequence from KOs. Three line of KOs, -3, -14 and -16 were obtained. In this thesis, -14 is used as KO. **(C)** HE-stained 5 μm section of testes from WT sibling and KO. In KO testes, no sperm (SP) was observed. Scale bar = 10 μm. **(D, E)** RT-qPCR of *sycp2* using WT, *its* mutant (its) and *sycp2* KO (KO). References were *actb1* (D) and *rps29*(E). Using both references, *its* mutant and *sycp2* KO showed significant reduction of *sycp2*. *its* mutant showed slightly higher expression compared to *sycp2* KO however, the difference was not statistically significant (n=5). Values represent the mean ±SD. **P<0.01, ***P< 0.001.

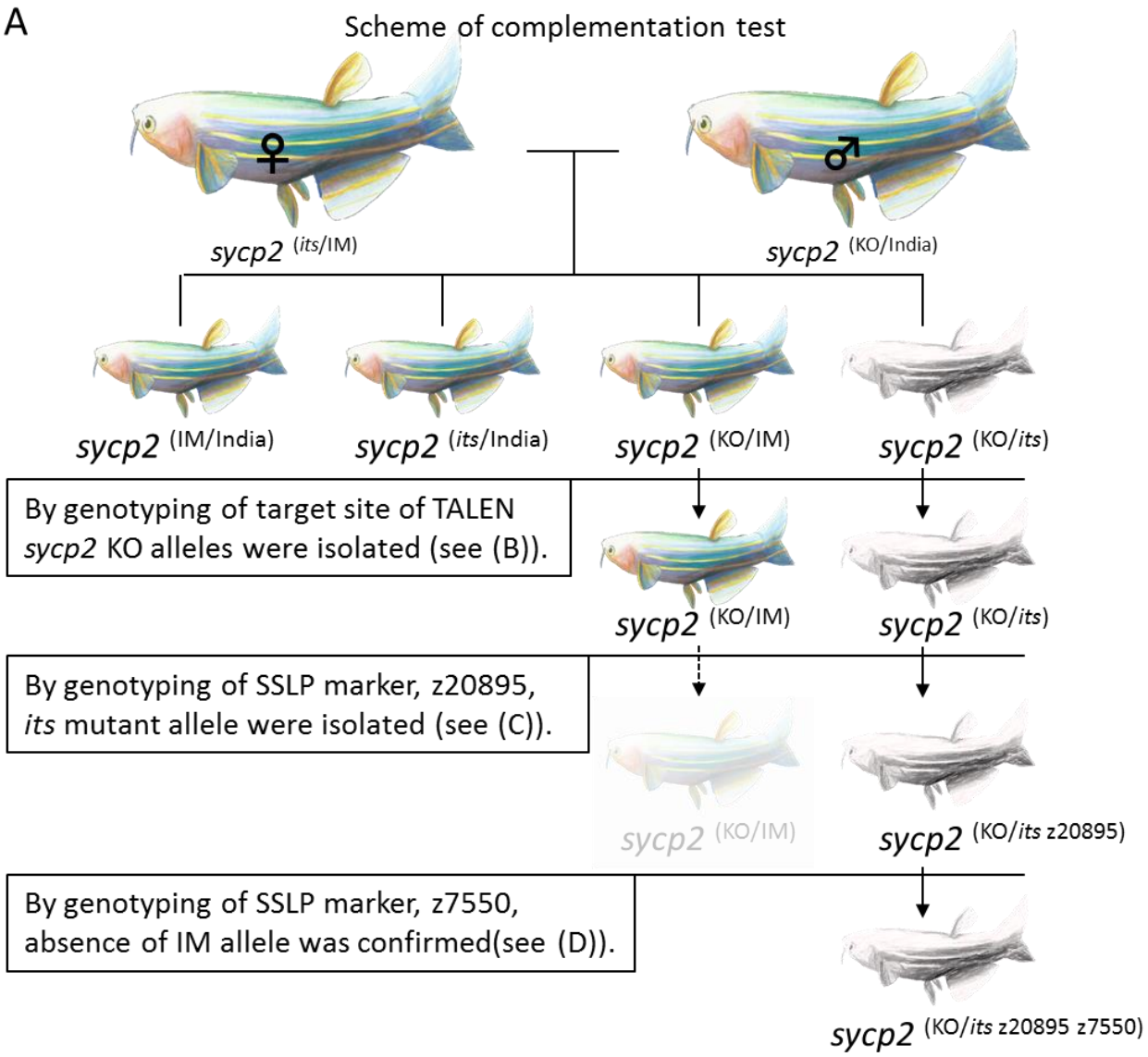
A
Scheme of complementation test
♀
♂
sycp2 (its/IM)
sycp2 (KO/India)
sycp2 (IM/India)
sycp2 (its/India)
sycp2 (KO/IM)
sycp2 (KO/its)
By genotyping of target site of TALEN sycp2 KO alleles were isolated (see (B)).
sycp2 (KO/IM)
sycp2 (KO/its)
By genotyping of SSLP marker, z20895, its mutant allele were isolated (see (C)).
sycp2 (KO/IM)
sycp2 (KO/its z20895)
By genotyping of SSLP marker, z7550, absence of IM allele was confirmed(see (D)).
sycp2 (KO/its z20895 z7550)

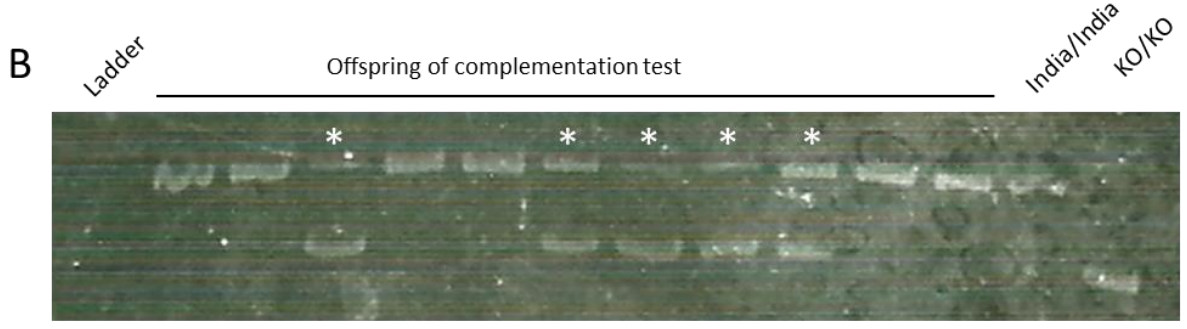
B
Ladder
Offspring of complementation test
India/India
KO/KO

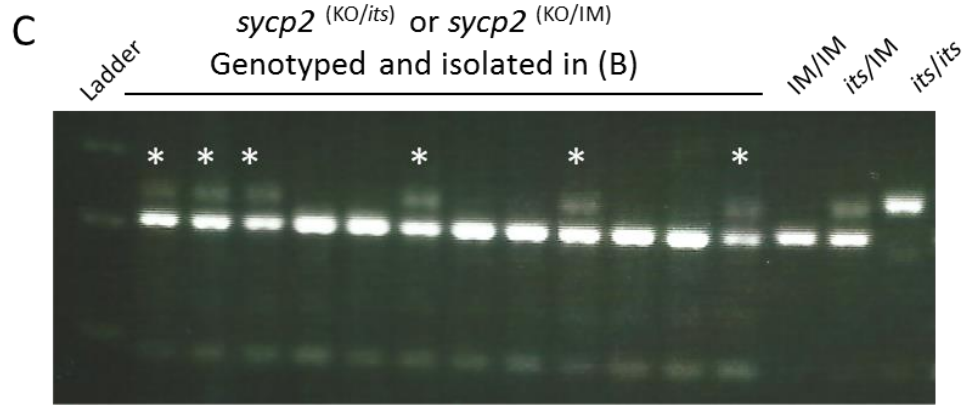
C
sycp2 (KO/its) or sycp2 (KO/IM)
Genotyped and isolated in (B)
Ladder
IM/IM
its/IM
its/its

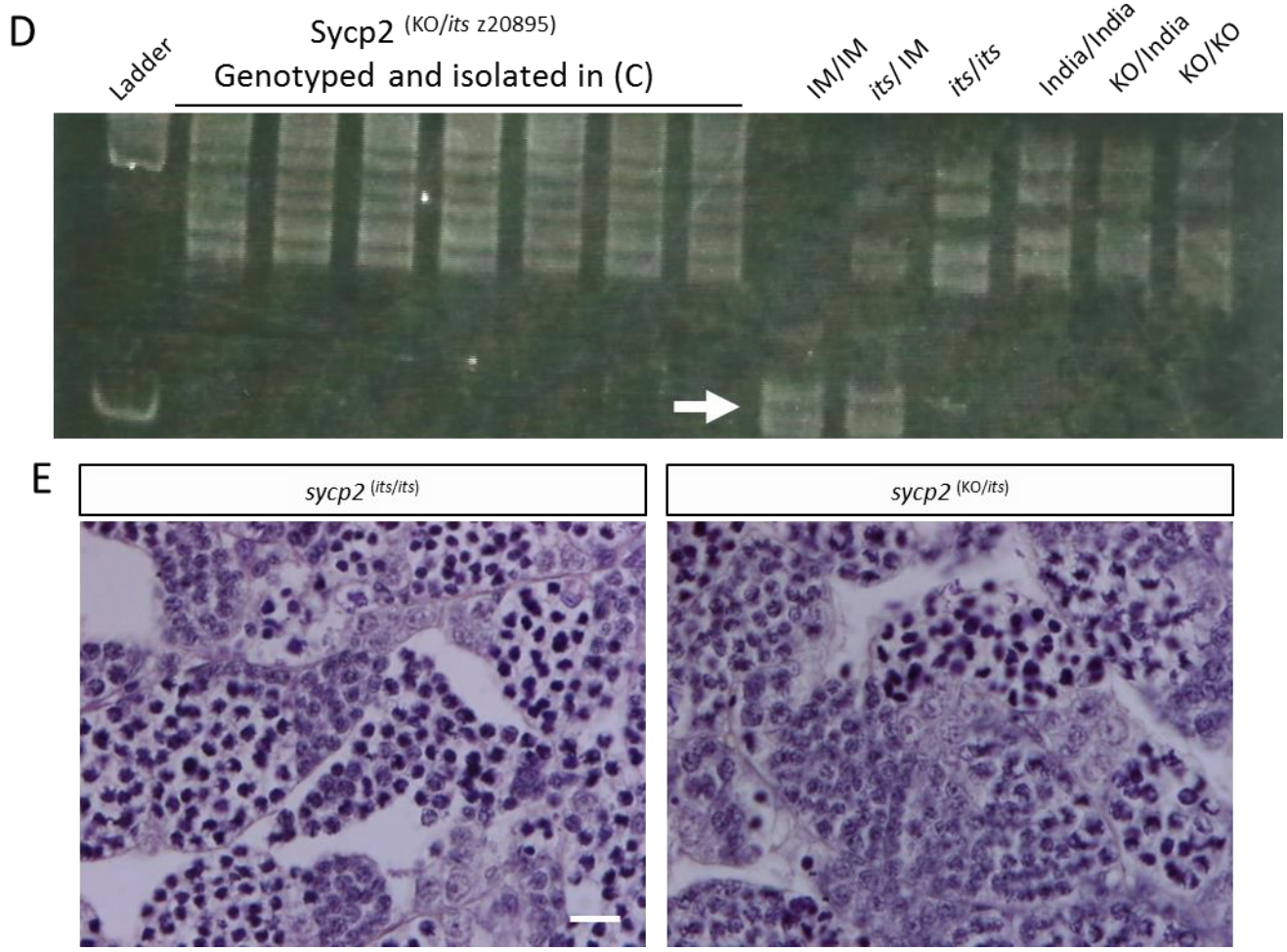

Figure 6.Complementation test of *its* mutant and *sycp2* KO (A) A scheme of complementation test. Heterozygous *its* mutant (*sycp2* $^{(its/IM)}$) and *sycp2* KO (*sycp2* $^{(KO/India)}$) are crossed. The genotype of offspring is IM/India, *its*/India, KO/IM or KO/*its*. From these fish, first, KO Alleles were isolated shown in (B). Second, its mutant allele were isolated shown in (C). Finally, absence of IM allele is confirmed shown in (D). **(B)** Genotyping of offspring using primers around target site of TALENs. Asterisks indicate fish contain KO allele. Note that KO allele show smaller size of band than WT. **(C)** Genotyping of fish heterozygous at KO site (*sycp2* $^{(KO/IM)}$ or *sycp2* $^{(KO/its)}$) isolated in (B) using SSLP marker z20895. Asterisks indicate fish contain *its* allele. **(D)** Genotyping of fish heterozygous at z20895 (*sycp2* $^{(KO/its\ z20895)}$) isolated in (C) using SSLP marker z7550. Note that all fish do not have IM allele (arrow). **(E)** HE-stained 5μm section of *its* homozygous mutant and offspring of complementation test which is heterozygous for both alleles. Both fish have no sperm in testes. Scale bar=10 μm

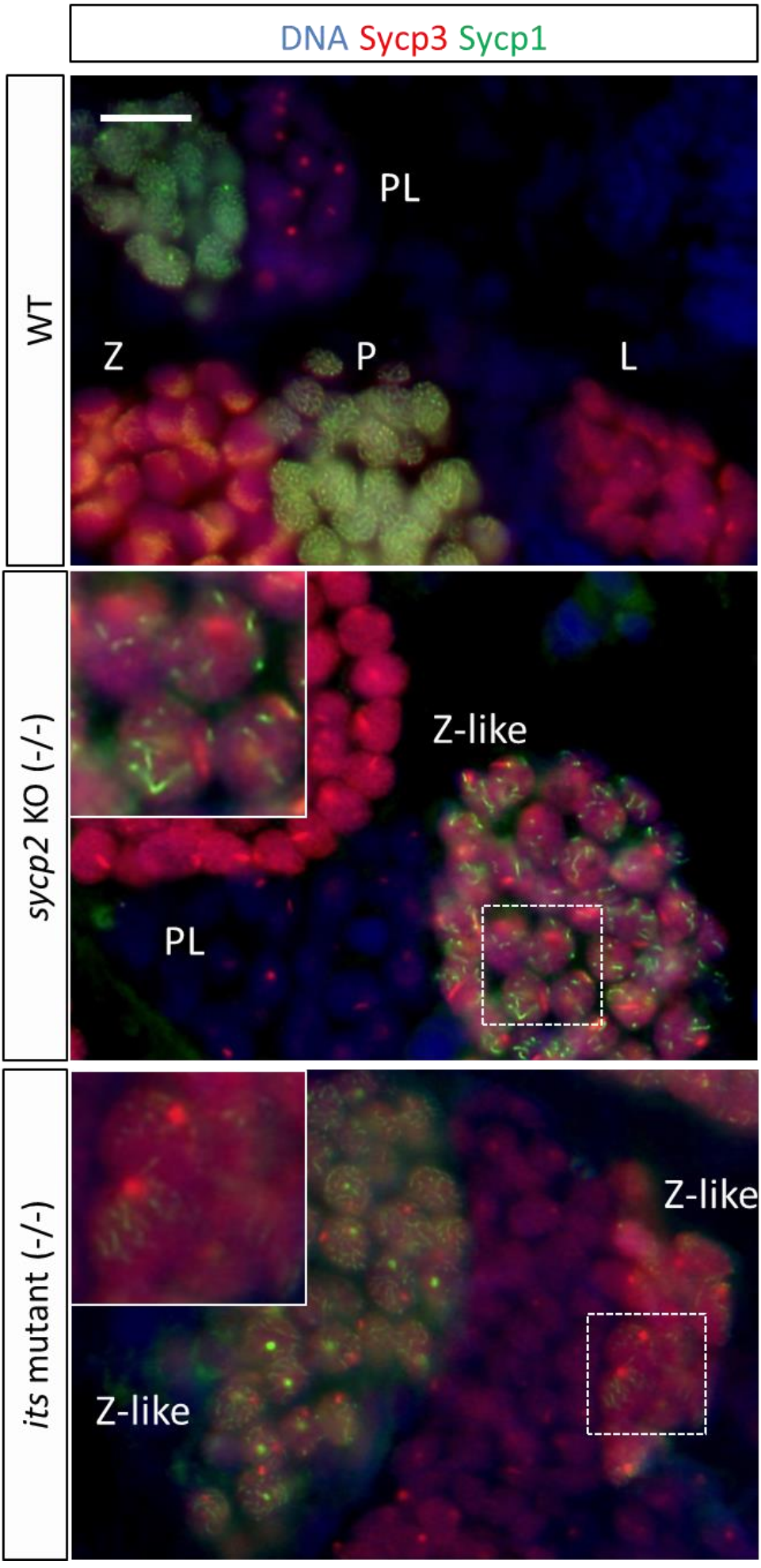
DNA Sycp3 Sycp1
WT
PL
Z
P
L
sycp2 KO (-/-)
Z-like
PL
its mutant (-/-)
Z-like
Z-like

Figure 7. *its* mutant showed mild defect in SCs formation compared with *sycp2* KO. Immunohistochemistry of Sycp3 and Sycp1 using 5μm paraffin embedded testes section of WT, *sycp2* KO and *its* mutant. WT showed all stages of prophase I, preleptotene (PL), leptotene (L), zygotene (Z) and pachytene (P). *sycp2* KO showed Zygotene-like (Z-like) phenotype which is aberrant short rod-like synapsis by Sycp1(inset). *its* mutant also showed zygotene-like phenotype, however, synapsis looked relatively highly formed compared with KO.Especially, spermatocytes in right show elongation-like synapsis from telomere bouquet (inset). Scale bar = 10 μm

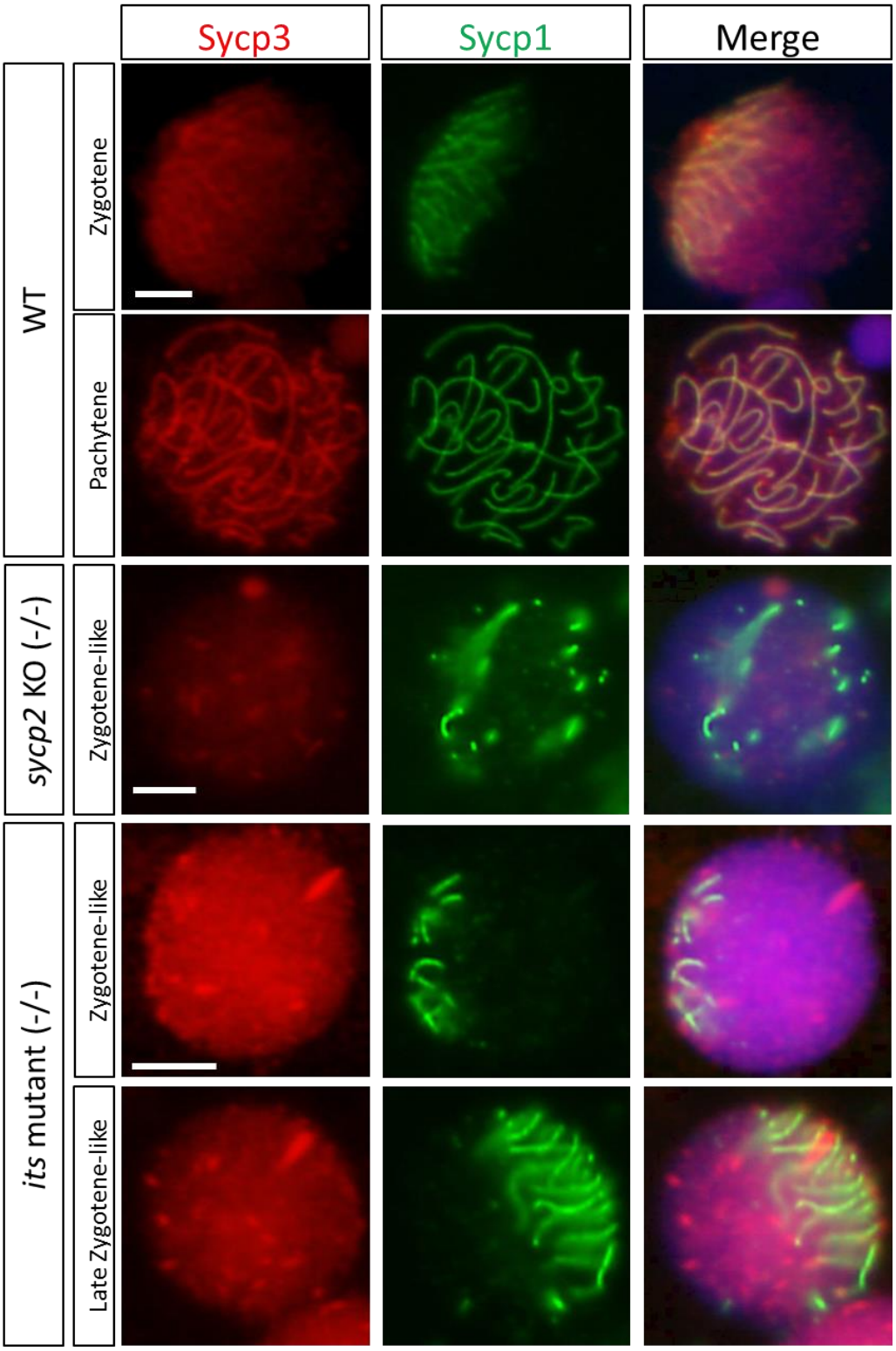

Figure 8. Synapsis from one pole of nuclei is maintained in *its* mutant.

Immunocytochemistry of Sycp3 and Sycp1 using spermatocyte spread. *sycp2* KO showed complete disruption of synapsis from one pole of nuclei while *its* mutant restore it. Scale bar=2.5 µm

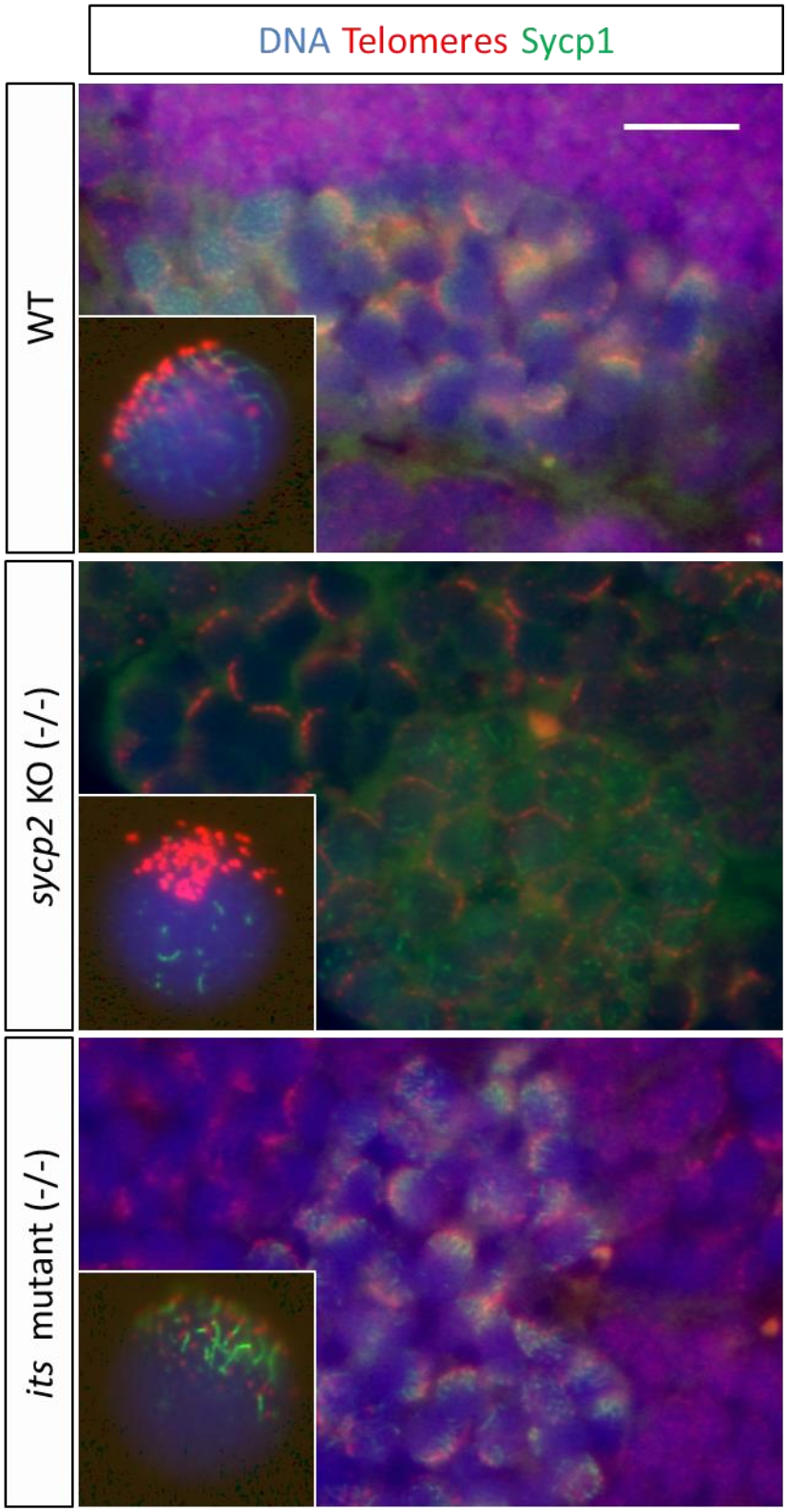

Figure 9. Synapsis from telomere bouquet is maintained in *its* mutant Combination of immunohistochemistry and telomere-FISH using 5μm paraffin embedded section and spermatocyte spread. Synapsis from one pole of nuclei in *its* mutant coincides with telomere bouquet same as WT. Inset indicate spermatocyte spread in zygotene(-like) stage from WT ,*its* mutant and *sycp2* KO. Scale bar = 10 μm

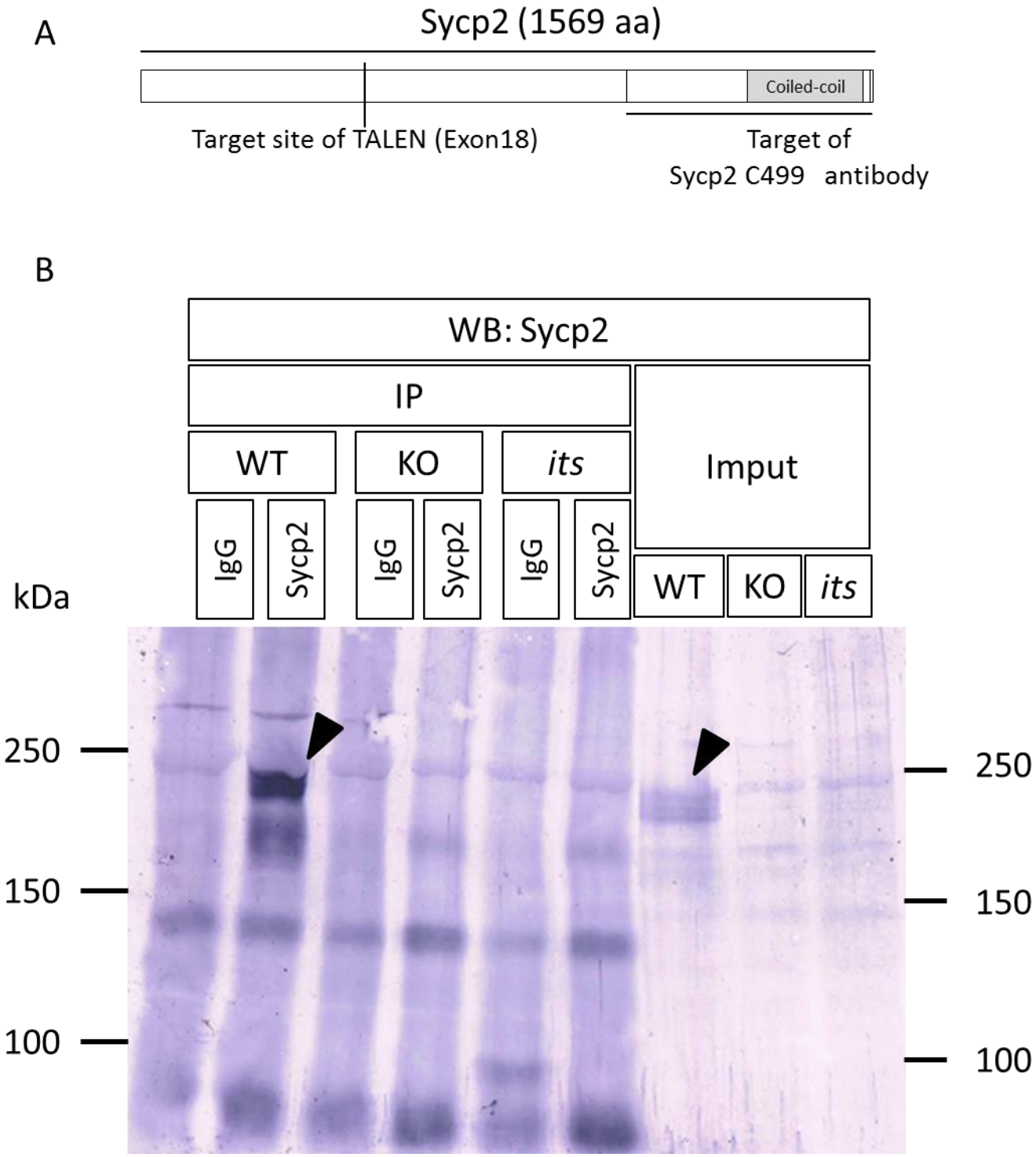

Figure 10. Immunoprecipitation of Sycp2 from testes lysetes of WT, *sycp2* KO and *its* mutant. (A) A schematic of target locus of anti-Sycp2C499 antibody. **(B)** Sycp2 protein is immunoprecipitated by guinea pig anti-Sycp2C499 antibody and protein A sepharose and detected by western blotting using same antibody. Sycp2 protein are successfully concentrated and only WT showed Sycp2 specific band (arrowhead).

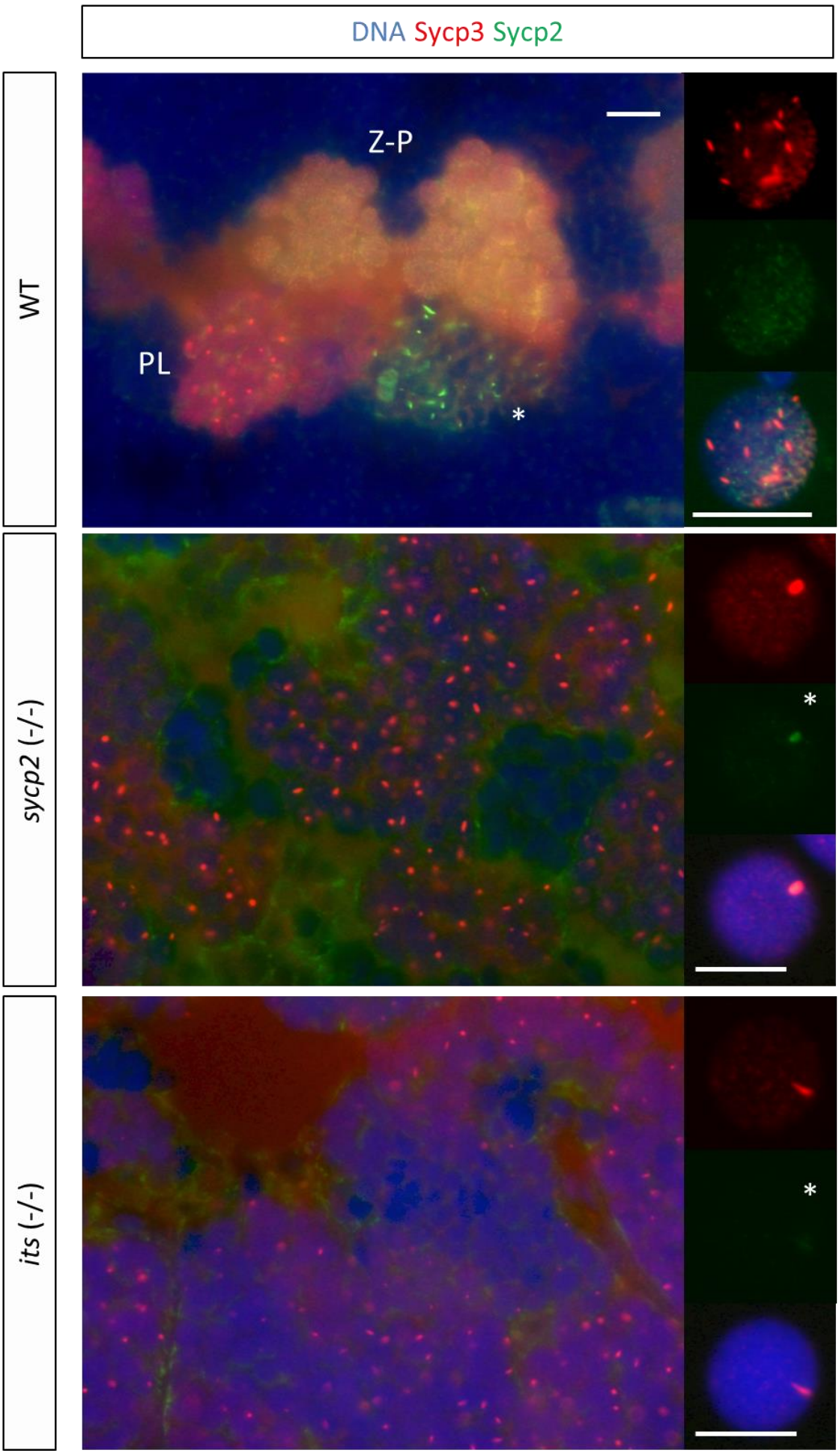
DNA Sycp3 Sycp2
WT
Z-P
PL
*
sycp2 (-/-)
*
its (-/-)
*

Figure 11. In *its* mutant testes, Sycp2 protein was not detected.

Immunohistochemistry of Sycp2 and Sycp3 using 5μm paraffin embedded section and spermatocyte spread from WT, *sycp2* KO and *its* mutant testes. In WT spermatocytes Sycp2 protein was detected in several cysts as SCs in zygotene-pachytene (Z-P) or as short thick fiber in unknown type of cyst (asterisk), but not in preleptotene (PL). In *sycp2* KO and *its* mutant, Sycp2 protein is not detected while most spermatocytes forms large aggregate like preleptotene. Scale bar = 10 μm Asterisk indicate the leak of fluorescence of Cy3.

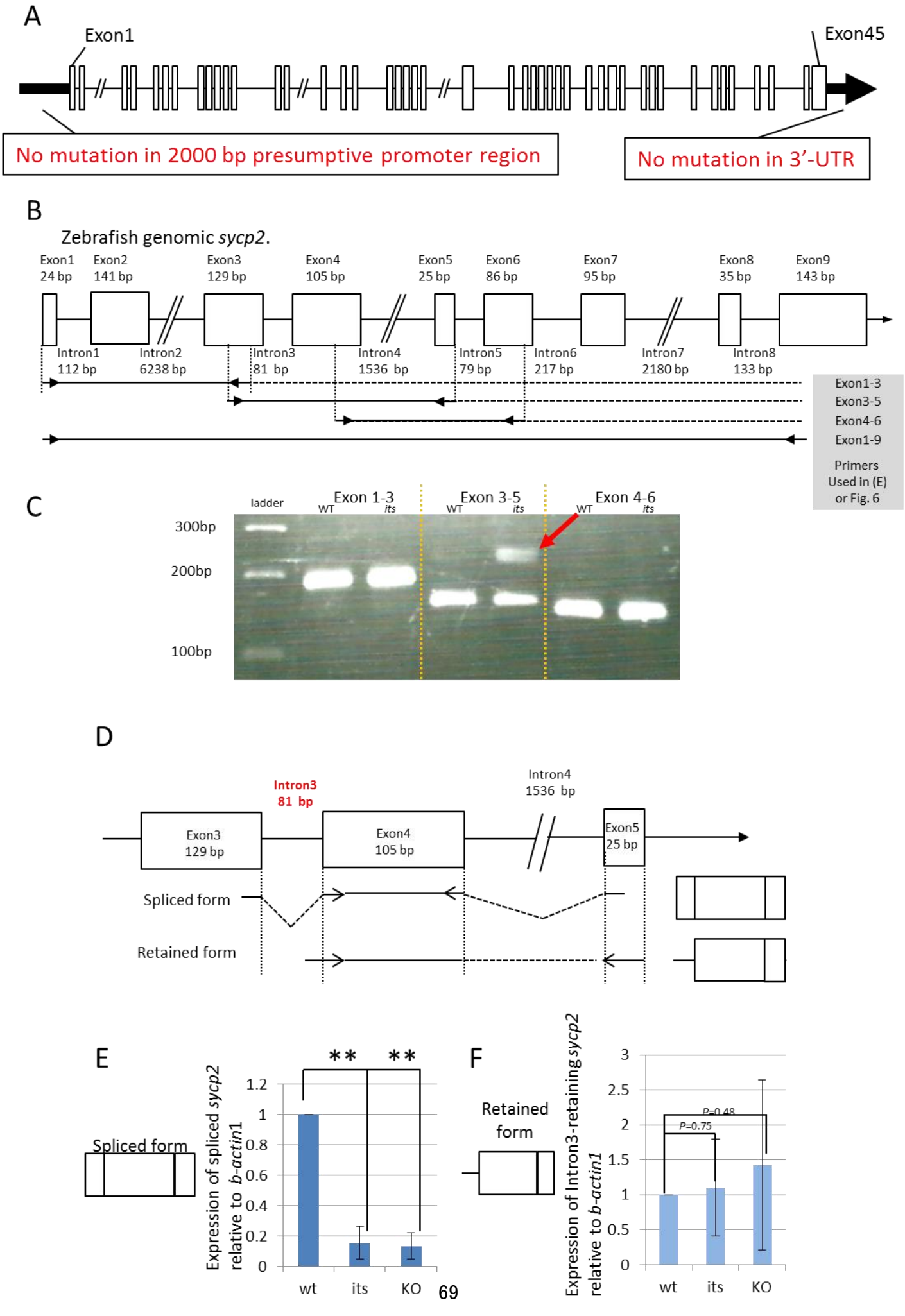
A
Exon1
Exon45
No mutation in 2000 bp presumptive promoter region
No mutation in 3'-UTR
B
Zebrafish genomic sycp2.
Exon1 24 bp
Exon2 141 bp
Exon3 129 bp
Exon4 105 bp
Exon5 25 bp
Exon6 86 bp
Exon7 95 bp
Exon8 35 bp
Exon9 143 bp
Intron1 112 bp
Intron2 6238 bp
Intron3 81 bp
Intron4 1536 bp
Intron5 79 bp
Intron6 217 bp
Intron7 2180 bp
Intron8 133 bp
Exon1-3
Exon3-5
Exon4-6
Exon1-9
Primers Used in (E) or Fig. 6
C
ladder
Exon 1-3
Exon 3-5
Exon 4-6
WT
its
300bp
200bp
100bp
D
Intron3 81 bp
Intron4 1536 bp
Exon3 129 bp
Exon4 105 bp
Exon5 25 bp
Spliced form
Retained form
E
Spliced form
Expression of spliced sycp2 relative to b-actin1
**
**
1.2
1
0.8
0.6
0.4
0.2
0
wt
its
KO
F
Retained form
Expression of Intron3-retaining sycp2 relative to b-actin1
P=0.48
P=0.75
3
2.5
2
1.5
1
0.5
0
wt
its
KO

Figure 12. RT-PCR of *sycp2* mRNA in *its* mutant. RT-PCR of *sycp2* mRNA was performed using various primers.**(A)** No mutation was found in presumptive promoter region and 3'-UTR. **(B)** A schematic of prier design used in (C) to analyze the splicing in 5' side of transcript. **(C)** RT-PCR analysis of 5' side of 5' side of *sycp2* transcript. Only exon3-5 of *its* mutant showed additional band indicating the retention of intron 3. **(D)** A schematic of primer design for intron3 spliced form and retained form of *sycp2* mRNA.**(E, F)** Quantification of intron3 spliced form (E) and retained form (F). The amount of spliced form was statistically significantly lower in *its* mutant and *sycp2* KO (E), while retained form was not (F). This indicate the retained form exist in equal frequency in testes of both WT and mutants. Values represent the mean ±SD. **P<0.01

A

sycp2 cDNA

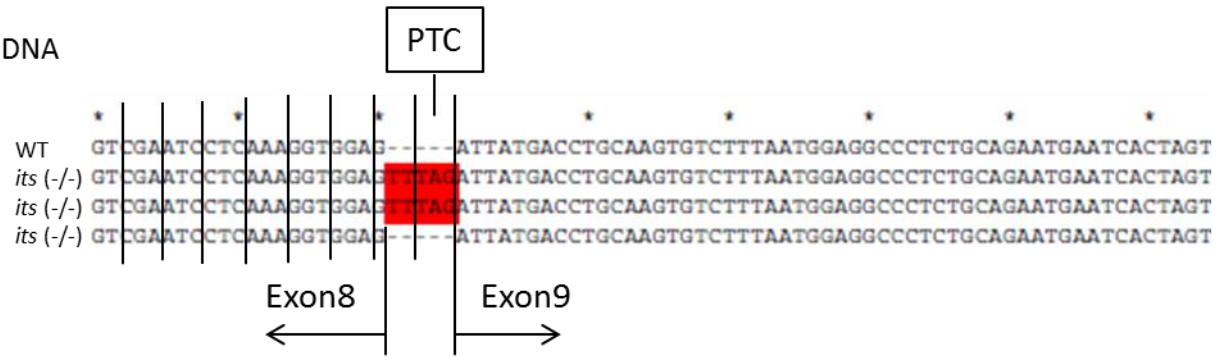

B

sycp2 (genomic)

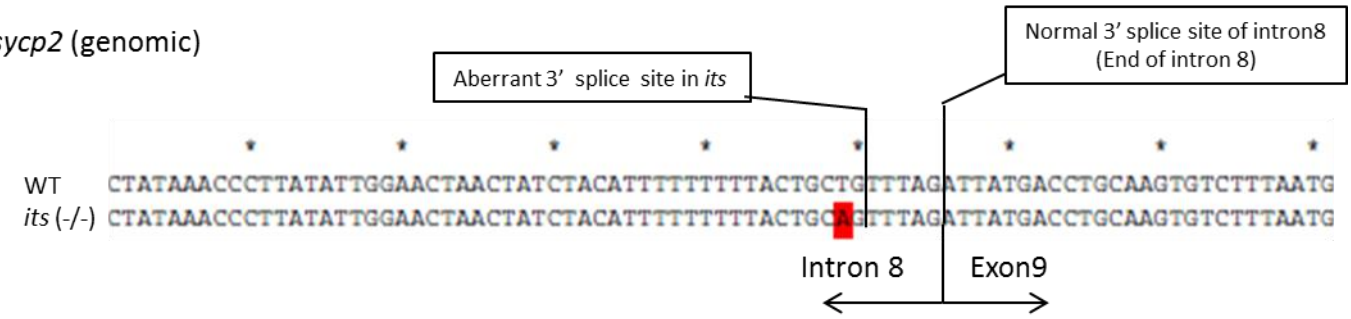

C

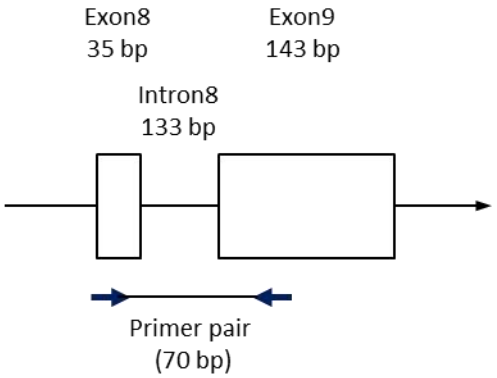

E

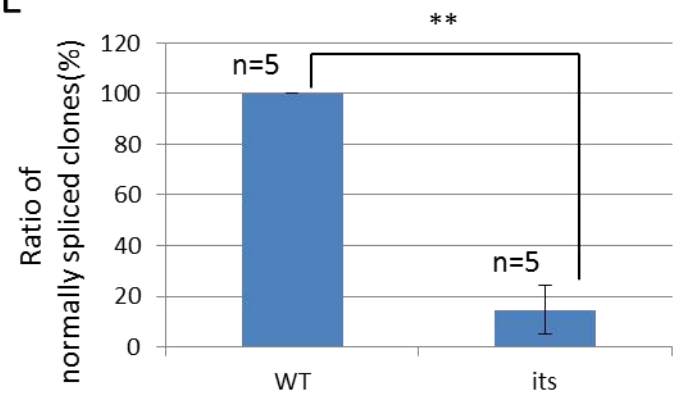

D

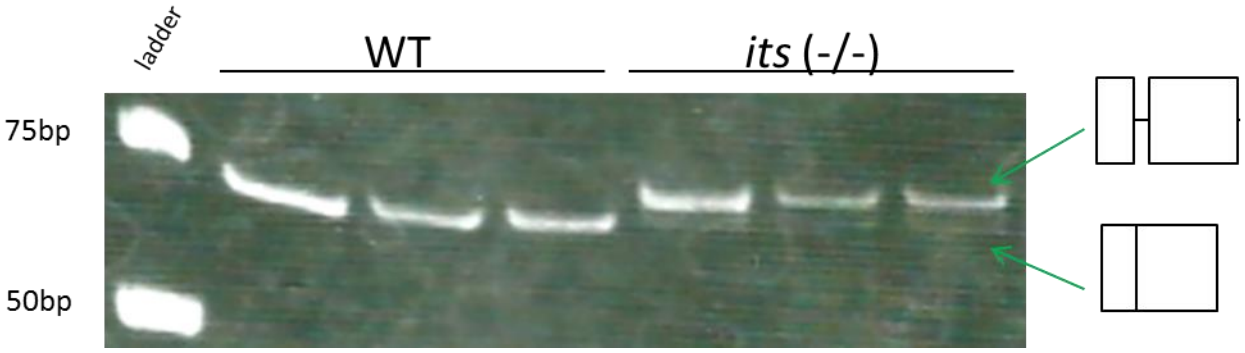

Figure 13. T to A substitution in intron8 of *its* mutant cause aberrant splicing. (A) Sequence around junction of exon8 and exon9 of *sycp2* cDNA from WT sibling and *its* homozygous mutant. *its* homozygous mutant have normal mRNA and aberrant mRNA with 5 bp insertion in exon junction. **(B)** Genomic sequence around junction of intron8 and exon9 from WT sibling and *its* homozygous mutant. *its* homozygous mutant have T to A substitution that can be aberrant 3'-splice sites. **(C)** A schematic of primer design around intron8. **(D)** RT-PCR using primers shown in (C). *its* homozygous mutant showed shifted band in addition to WT band. **(E)** The ratio of normally spliced cDNA fragments obtained in (D). *its* homozygous mutant showed statistically significant reduction of normally spliced cDNA to 10 %. Values represent the mean ±SD. **P<0.01

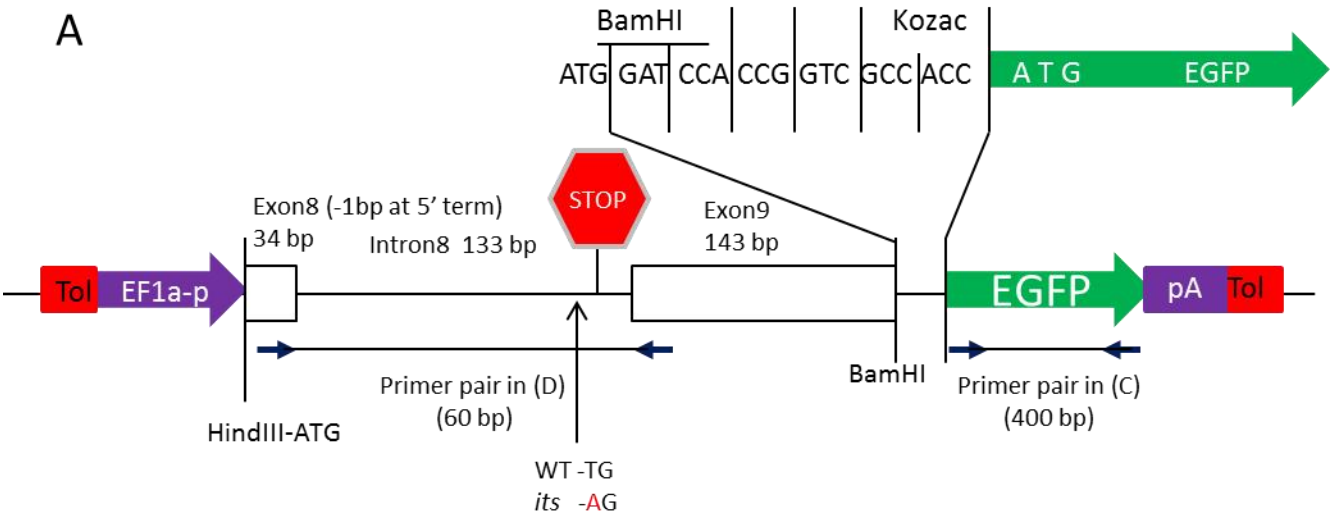
A
BamHI
Kozac
ATG GAT CCA CCG GTC GCC ACC
A T G
EGFP
STOP
Exon8 (-1bp at 5' term)
34 bp
Intron8 133 bp
Exon9
143 bp
Tol
EF1a-p
EGFP
pA
Tol
BamHI
Primer pair in (D)
(60 bp)
Primer pair in (C)
(400 bp)
HindIII-ATG
WT -TG
its -AG

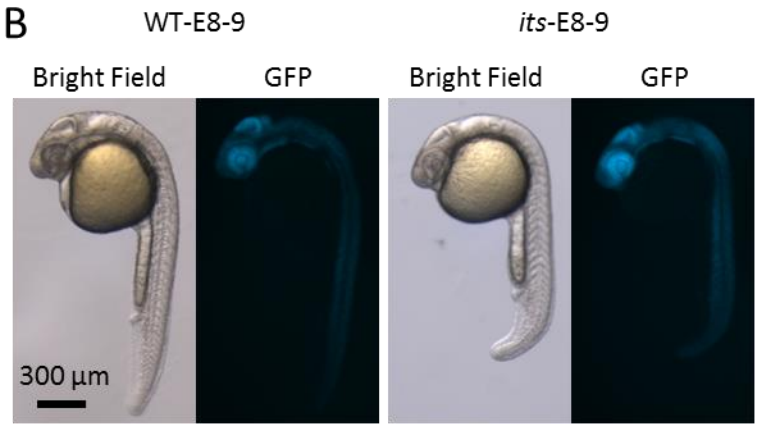
B
WT-E8-9
its-E8-9
Bright Field
GFP
Bright Field
GFP
300 µm

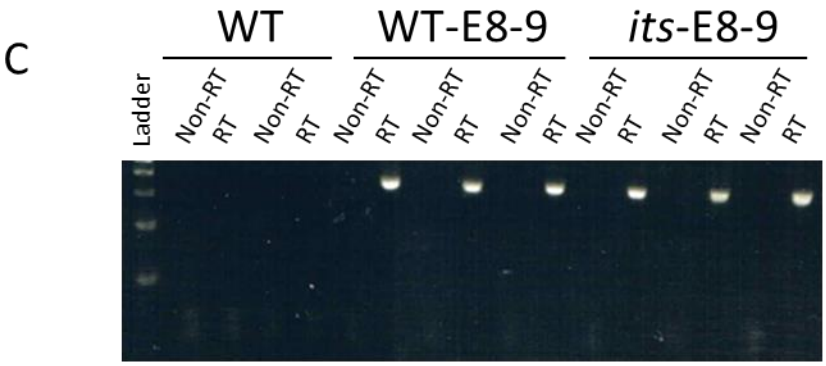
C
WT
WT-E8-9
its-E8-9
Ladder
Non-RT
RT
Non-RT
RT
Non-RT
RT
Non-RT
RT
Non-RT
RT
Non-RT
RT
Non-RT
RT

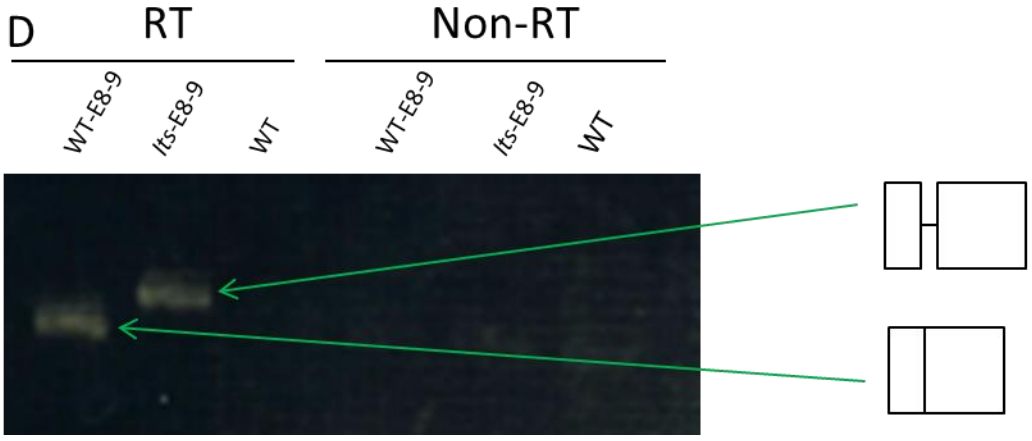
D
RT
Non-RT
WT-E8-9
its-E8-9
WT
WT-E8-9
its-E8-9
WT

Figure 14 *its* mutation result in aberrant splicing in WT background. (A) A schematic of design of minigene containing exon8, intron8 and exon9. Each vertial bars inserted every 3bp in top indicate codon frame. Primers used in (C) are indicated below exon8 and exon9. **(B)** GFP fluorescence of transgenic fish with minigenes. Both WT-E8-9 and *its*-E8-9 showed fluorescence by the presense of kozac sequence. Scale bar = 300 μm **(C,D)** RT-PCR analysis of caudal fin cDNA from WT, WT-E8-9 and *its*-E8-9. Primers are shown in (A). In WT background which did not have minigene **(C),** *its*-E8-9 showed shifted band while WT showed normal 60 bp band**(D).**

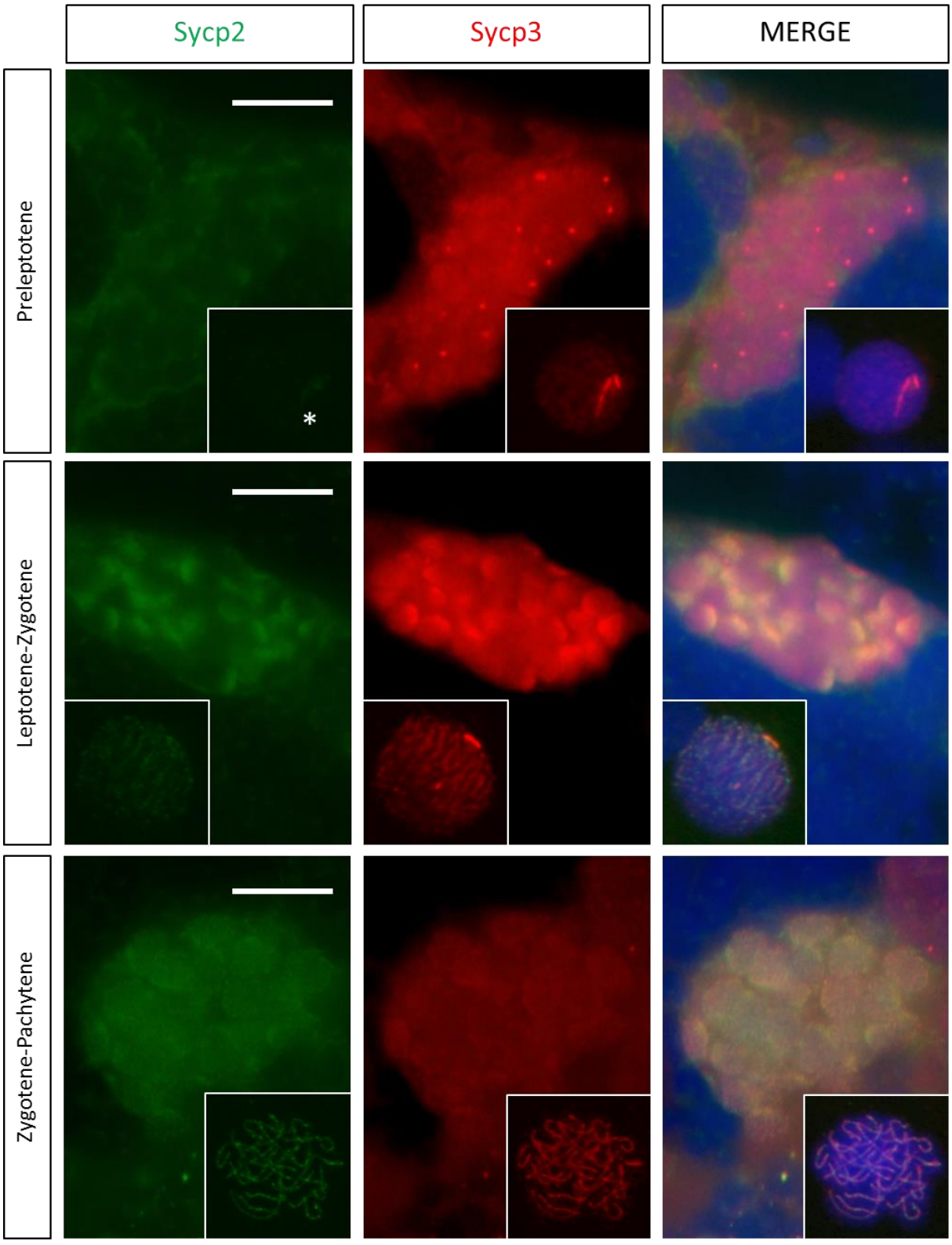

Figure 15. In preleptotene spermatocytes, Sycp2 do not exists in nucleus.

Immunohistochemistry of Sycp2 and Sycp3 using 5μm paraffin embedded section of WT testes. In preleptotene spermatocytes which Sycp3 form large aggregate in nucleus, Sycp2 are not detected in nucleus. In later stage, both proteins co-localized.

Scale bar = 10 μm Asterisks indicate the leak of fluorescence of Cy3.

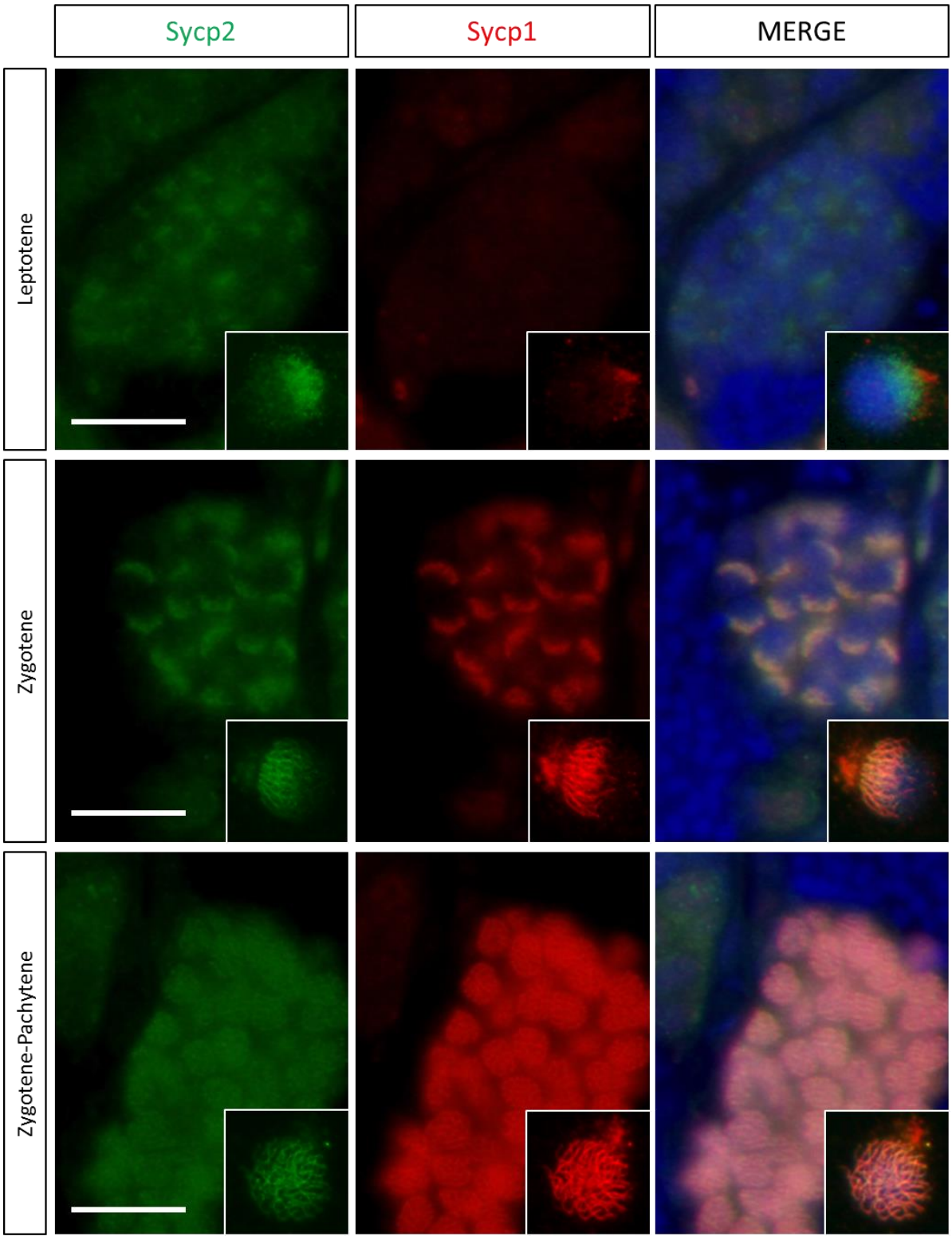

Figure 16 .Co-localization of Sycp2 and Sycp1. Immunohistochemistry of Sycp2 and Sycp1 using 5μm paraffin embedded section of WT testes. Inset indicate immunocytochemystery on spermatocyte spread. In leptotene spermatocytes which Sycp2 localize one pole of nuclei, Sycp1 is not detected. After zygotene which synapsis by Sycp1 starts, Sycp2 co-localized with Sycp1. Scale bar = 10 μm

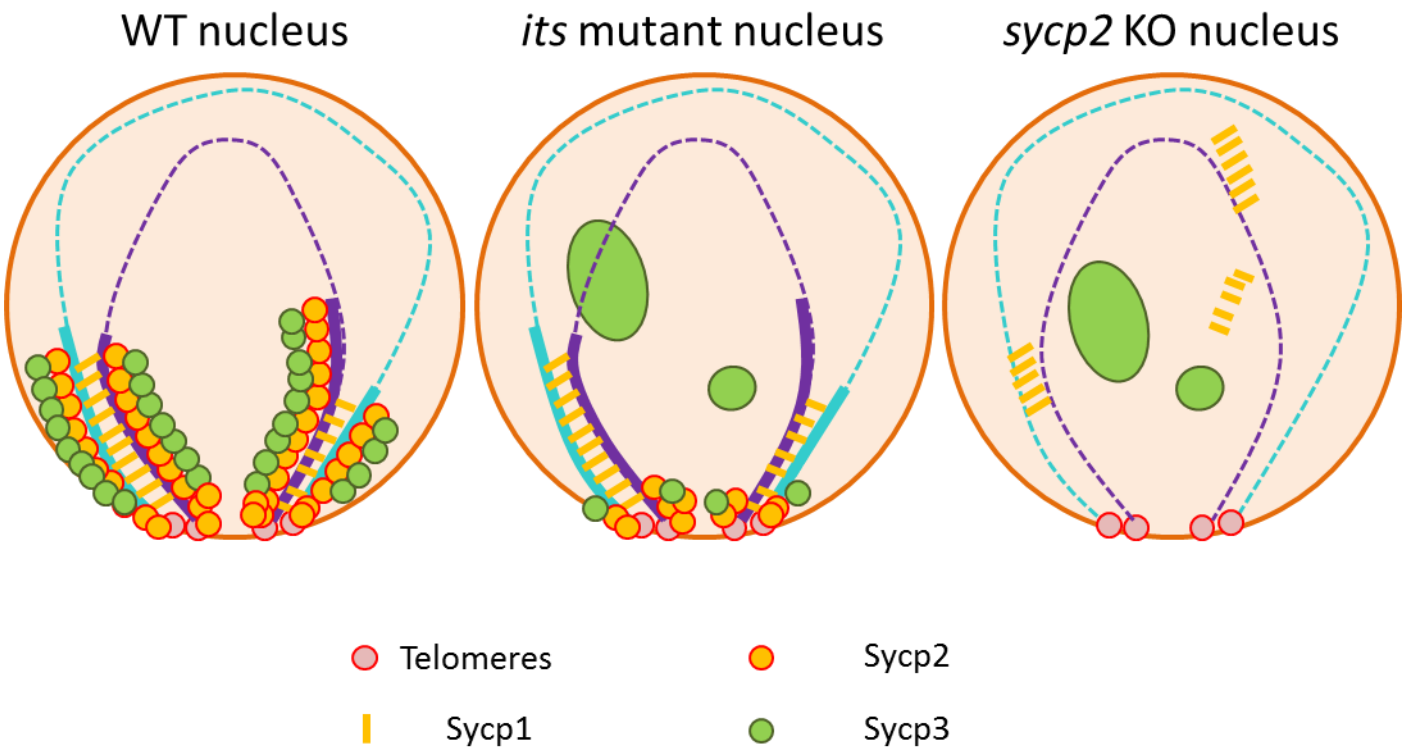

Figure 17. Meiotic chromosome architecture in zebrafish WT, *its* mutant and *sycp2* KO. The model of meiotic chromosome architecture shown in this study. In WT, SCs formation starts from telomrere bouquet. In *its* mutant, small amount of Sycp2 protein must be translated and localize to telomere and synapsis by Sycp1 are maintained while most Sycp3 protein thought to be aggregated. In *sycp2* KO, no Sycp2 protein exists in nucleus. Sycp1 form aberrant SCs-like structure and Sycp3 only form aggregates.

Table.1 The genes in causal genomic locus of *its* mutant in zebrafish chromosome 23.

Danio rerio Genome (Annotation Release 104)

#Chromosome: 23

##########

#Map: genes

#Region: 7,915,563..13,456,320

#start	stop	Symbol	Orientatio	Description	
7823271	8016386	myt1b	−	mRNA	myelin transcription factor 1b
8261037	8263621	LOC571123	+	best RefSeq	Gpr7
8360928	8449812	oprl1	−	best RefSeq	opiate receptor-like 1
8651470	8658156	LOC100329490	+	rnaseq	uncharacterized LOC100329490
8671798	8765272	rgs19	+	best RefSeq	regulator of G protein signaling 19
8783980	8798094	tcea2	−	best RefSeq	transcription elongation factor A (SII), 2
8852857	8865784	sox18	+	mRNA	SRY (sex determining region Y)-box 18
9054198	9080056	xkr7	+	best RefSeq	XK, Kell blood group complex subunit-related family, member 7
9100487	9146836	ccm2l	+	mRNA	cerebral cavernous malformation 2-like
9153232	9203559	cables2b	+	mRNA	Cdk5 and Abl enzyme substrate 2b
9285490	9293608	rps21	+	best RefSeq	ribosomal protein S21
9295570	9353479	acss2	+	best RefSeq	acyl-CoA synthetase short chain family member 2
9450226	9460078	LOC103909657	+	rnaseq	uncharacterized LOC103909657
9465301	9557132	soga1	−	mRNA	suppressor of glucose, autophagy associated 1
9573568	9616997	osbpl2b	+	best RefSeq	oxysterol binding protein-like 2b
9625997	9632336	adrm1	+	best RefSeq	adhesion regulating molecule 1
9632364	9833782	lama5	−	best RefSeq	laminin, alpha 5
9859709	9872618	mapre1b	−	best RefSeq	microtubule-associated protein, RP/EB family, member 1b
9874660	9928661	prkcbp1l	−	best RefSeq	protein kinase C binding protein 1, like
9928760	9959953	LOC103909658	−	rnaseq	uncharacterized LOC103909658
9932520	9954360	slc16a7	+	best RefSeq	solute carrier family 16, member 7 (monocarboxylic acid transporter 2)
9973841	9990624	si:ch211-220i18.4	−	mRNA	SRSF protein kinase 3-like
10003268	10202425	plxnb1a	−	mRNA	plexin b1a
10004701	10014383	LOC103909659	+	rnaseq	uncharacterized LOC103909659
10211572	10227901	zgc:171775	+	best RefSeq	zgc:171775
10238228	10242467	krt5	−	best RefSeq	keratin 5
10314656	10319271	krt8	−	best RefSeq	keratin 8
10412886	10416783	krt18	+	best RefSeq	keratin 18
10417951	10421158	si:ch211-133j6.3	+	mRNA	
10461918	10514513	eif4ba	+	best RefSeq	eukaryotic translation initiation factor 4Ba
10535011	10652291	tns2a	+	protein	tensin 2a
10690387	10693102	LOC101882287	−	mRNA	uncharacterized LOC101882287
10693182	10696454	LOC101882326	−	rnaseq	uncharacterized LOC101882326
10703039	10787772	foxp1a	−	best RefSeq	forkhead box P1a
10789072	10810297	eif4e3	−	best RefSeq	eukaryotic translation initiation factor 4E family member 3
10811636	10817912	LOC101882372	+	rnaseq	uncharacterized LOC101882372
10827714	10851430	rybpa	−	best RefSeq	RING1 and YY1 binding protein a
10866055	10866776	LOC103909660	−	rnaseq	uncharacterized LOC103909660
10866775	10868441	LOC101882482	−	rnaseq	uncharacterized LOC101882482
10870216	10892027	ppp4r2a	+	best RefSeq	protein phosphatase 4, regulatory subunit 2a
10892602	10979598	pdzrn3a	−	protein	PDZ domain containing RING finger 3a
11071014	11289788	cntn3a.2	−	protein	contactin 3a, tandem duplicate 2
11350716	11513777	chl1a	+	best RefSeq	cell adhesion molecule L1-like a
11407634	11409706	LOC101882732	−	rnaseq	uncharacterized LOC101882732
11616967	11617890	LOC103909662	−	protein	putative nuclease HARBI1 pseudogene
11734232	11927377	cntn3a.1	+	mRNA	contactin 3a, tandem duplicate 1
11929250	12080046	si:dkey-178k16.1	−	mRNA	uncharacterized protein im:7155308
12082747	12085641	LOC101883160	−	rnaseq	uncharacterized LOC101883160
12138010	12173369	edn3b	+	mRNA	endothelin-3
12199817	12215505	ttll9	+	best RefSeq	tubulin tyrosine ligase-like family, member 9
12219240	12224200	fam217b	−	mRNA	family with sequence similarity 217, member B
12226011	12227776	ppp1r3da	+	best RefSeq	protein phosphatase 1, regulatory subunit 3Da
12262819	12272459	LOC103909663	+	mRNA	uncharacterized LOC103909663
12272461	12272989	LOC103909661	+	rnaseq	uncharacterized LOC103909661
12275157	12293355	sycp2	+	mRNA	synaptonemal complex protein 2
12297803	12410794	phactr3a	−	best RefSeq	phosphatase and actin regulator 3a
12426924	12479659	pigt	+	mRNA	phosphatidylinositol glycan anchor biosynthesis, class T
12483639	12488864	wfdc2	−	mRNA	WAP four-disulfide core domain 2
12493752	12518730	snx21	−	best RefSeq	sorting nexin family member 21
12518346	12551445	si:ch211-153a8.4	+	mRNA	si:ch211-153a8.4
12610201	12677849	si:zfos-452g4.1	+	mRNA	si:zfos-452g4.1
12705806	12706645	LOC103909664	+	rnaseq	uncharacterized LOC103909664
12710413	12711152	LOC103909665	+	rnaseq	uncharacterized LOC103909665
12771707	12772262	LOC103909666	+	rnaseq	uncharacterized LOC103909666
12816961	12847024	LOC100535655	−	protein	CD209 antigen-like protein 2
12918850	12919344	LOC101885492	+	rnaseq	uncharacterized LOC101885492
12926352	13032164	si:dkey-96f10.1	−	mRNA	6-phosphofructo-2-kinase/fructose-2,6-biphosphatase-like
12942894	12944337	LOC103909667	+	rnaseq	uncharacterized LOC103909667
13072863	13074170	LOC101885711	+	rnaseq	uncharacterized LOC101885711
13084023	13141499	smc1al	+	best RefSeq	structural maintenance of chromosomes 1A, like
13144339	13157054	ndnl2	−	best RefSeq	necdin-like 2
13159858	13177419	si:dkey-150i13.2	+	mRNA	
13203907	13205302	LOC103909668	+	rnaseq	uncharacterized LOC103909668
13237399	13250605	LOC101882265	−	protein	paraneoplastic antigen Ma1 homolog
13367908	13576786	samd10b	+	mRNA	sterile alpha motif domain containing 10b
13445832	13453895	LOC101885831	+	rnaseq	uncharacterized LOC101885831
13447497	13450546	LOC101882462	+	rnaseq	uncharacterized LOC101882462

Table.2 Sterility of *sycp2* KO

Crossed pairs	Number of matings(tested fish)	Total eggs obtained	Fertilization ratio(%)
WT♂ × WT♀	4	375	249 (66.4)
sycp2 −/− ♂× WT♀	6	825	0 (0)

Table.3 *sycp2* KO do not complement the phenotype of *its* mutant

Crossed pairs	Number of matings(tested fish)	Total eggs obtained	Fertilization ratio(%)
WT♂ × WT♀	1	239	227(94.9)
its/sycp2 (IM+/India−) ♂× WT♀	1	391	123(31.4)
its/sycp2 (Tu−/India−) ♂× WT♀	5	1785	0(0)